Chromium isotope fractionation during subduction-related metamorphism, black shale weathering, and hydrothermal alteration

Xiangli Wang[1*], Noah J. Planavsky[1], Christopher T. Reinhard[2], Huijuan Zou[1], Jay J. Ague[1], Yuanbao Wu[3], Benjamin C. Gill[4], Esther M. Schwarzenbach[4], Bernhard Peucker-Ehrenbrink[5]

[1] Yale University, Department of Geology and Geophysics, New Haven, Connecticut, USA; [2]Georgia Institute of Technology, School of Earth and Atmospheric Sciences, Atlanta, Georgia, USA; [3]China University of Geosciences, Faculty of Earth Sciences, Wuhan, Hubei, China; [4]Virginia Polytechnic Institute and State University, Blacksburg, VA, USA; [5]Woods Hole Oceanographic Institution, Woods Hole, MA, USA

*Corresponding author: xiangli.wang@yale.edu. 210 Whitney Ave, New Haven CT 06511.

ABSTRACT. Chromium (Cr) isotopes are an emerging proxy for redox processes at Earth's surface. However, many geological reservoirs and isotope fractionation processes are still not well understood. The purpose of this contribution is to move forward our understanding of (1) Earth's high temperature Cr isotope inventory and (2) Cr isotope fractionations during subduction-related metamorphism, black shale weathering and hydrothermal alteration. The examined basalts and their metamorphosed equivalents yielded δ^{53}Cr values falling within a narrow range of -0.12±0.13‰ (2SD, n=30), consistent with the previously reported range for the bulk silicate Earth (BSE). Compilations of currently available data for fresh silicate rocks (43 samples), metamorphosed silicate rocks (50 samples), and mantle chromites (39 samples) give δ^{53}Cr values of -0.13±0.13‰, -0.11±0.13‰, and -0.07±0.13‰, respectively. Although the number of high-temperature samples analyzed has tripled, the originally proposed BSE range appears robust. This suggests very limited Cr isotope fractionation under high temperature conditions. Additionally, in a highly altered metacarbonate transect that is representative of fluid-rich regional metamorphism,

we did not find resolvable variations in $\delta^{53}Cr$, despite significant loss of Cr. This work suggests that primary Cr isotope signatures may be preserved even in instances of intense metamorphic alteration at relatively high fluid-rock ratios. Oxidative weathering of black shale at low pH creates isotopically heavy mobile Cr(VI). However, a significant proportion of the Cr(VI) is apparently immobilized near the weathering surface, leading to local enrichment of isotopically heavy Cr ($\delta^{53}Cr$ values up to ~0.5‰). The observed large Cr isotope variation in the black shale weathering profile provides indirect evidence for active manganese oxide formation, which is primarily controlled by microbial activity. Lastly, we found widely variable $\delta^{53}Cr$ (-0.2‰ to 0.6‰) values in highly serpentinized peridotites from ocean drilling program drill cores and outcropping ophiolite sequences. The isotopically heavy serpentinites are most easily explained through a multi-stage alteration processes: Cr loss from the host rock under oxidizing conditions, followed by Cr enrichment under sulfate reducing conditions. In contrast, Cr isotope variability is limited in mildly altered mafic oceanic crust.

Keywords: Chromium isotopes, redox proxies, metamorphism, subduction, hydrothermal alteration, black shale weathering

1. Introduction

Chromium (Cr) isotopes (with abundances of 2.36% ^{54}Cr, 9.50% ^{53}Cr, 83.79% ^{52}Cr, 4.35% ^{50}Cr) have wide utility for tracking planetary formation, environmental contamination, and paleoenvironmental evolution. Over the past few decades, studies have utilized Cr isotope anomalies in different planetary materials to study spatial and/or temporal heterogeneities in the solar system (Birck and Allègre, 1984; Papanastassiou, 1986; Rotaru et al., 1992; Podosek et al., 1997; Shukolyukov and Lugmair, 2006; Trinquier et al., 2007; Qin et al., 2011). In addition, there

has been extensive work on using Cr isotopes to quantify the attenuation of environmental Cr contamination (Ellis et al., 2002; Wanner et al., 2011; Izbicki et al., 2012). More recently, there has been a surge of interest in using Cr isotopes as a paleoredox proxy (e.g., Frei et al., 2009; Crowe et al., 2013; Planavsky et al., 2014; Reinhard et al., 2014).

Chromium has two major valence states in nature: Reduced, trivalent Cr (denoted as Cr(III) hereafter) and oxidized, hexavalent Cr (denoted as Cr(VI) hereafter). At circumneutral pH, Cr(III) is insoluble and is a trace nutrient, while Cr(VI) is soluble and carcinogenic (Rai et al., 1989). Therefore, *in-situ* reduction of Cr(VI) to Cr(III) can serve as a means of remediating Cr(VI) contamination. In Earth's early history, before the emergence of oxygenic photosynthesis, Cr was likely present almost exclusively as Cr(III) in rocks. After the advent of oxygenic photosynthesis, local and eventually global oxygenated environments passed a critical threshold required for Cr(III) oxidation to Cr(VI), in a process likely linked to manganese redox cycling (Eary and Rai, 1987; Fendorf and Zasoski, 1992; Frei et al., 2009). The oxidized Cr(VI) is carried to the oceans as dissolved oxyanion species and eventually deposited in sedimentary rocks, either as Cr(VI) via adsorption or as Cr(III), typically via reduction by reductants such as ferrous iron and sulfides (Eary and Rai, 1987; Fendorf and Li, 1996; Pettine et al., 1998; Kim et al., 2001). Use of the Cr isotope system as a redox proxy is grounded in the notion that there is up to ~6‰ Cr isotope fractionation during reactions involving electron transfers (Ellis et al., 2002; Schauble et al., 2004; Zink et al., 2010; Wang et al., 2015a), but insignificant Cr isotope fractionations during non-redox-dependent reactions (e.g., Ellis et al., 2004). Studies on modern basaltic weathering profiles have found that isotopically heavy Cr is oxidatively mobilized into rivers, leaving isotopically light Cr in the weathered basalt (e.g., Frei and Polat, 2012). Building on this framework, Cr isotopes have

provided a new view of Earth's ocean-atmosphere redox evolution (Frei et al., 2009; Crowe et al., 2013; Planavsky et al., 2014).

Despite the significant potential of Cr isotopes as a redox proxy, there are several notable gaps in current knowledge. The purpose of this contribution is to examine a series of currently unresolved or poorly constrained questions that affect the use of the Cr isotope system as a paleoredox proxy. First, for all Cr isotope work, it is necessary to establish a robust estimate of the Cr isotope inventory of the solid Earth. Only a few studies have been conducted in the past few years for this purpose. For instance, Schoenberg et al. (2008) and Farkas et al. (2013) proposed bulk silicate Earth (BSE) $\delta^{53}Cr$ ($^{53}Cr/^{52}Cr$ relative to SRM 979) values of -0.124±0.101‰ and -0.079±0.129‰, respectively. Moynier et al. (2011) reported a bulk Earth (BE) $\delta^{53}Cr$ value of -0.32±0.05‰, which is about 0.2‰ lighter than the BSE value. The apparent difference between BE and BSE, and its potential implications for planetary differentiation, provides motivation to expand our current knowledge of the high-T Cr isotope inventory. For this purpose, we explored the $\delta^{53}Cr$ systematics of a range of basalt samples (both alkaline and tholeiitic) from different localities.

Second, Cr isotopic systematics in Archean rocks have been used to investigate the earliest emergence of oxygenic photosynthesis (Frei et al., 2009; Crowe et al., 2013). However, most Archean rocks have been subject to various grades of metamorphism. This provides a strong impetus to investigate the magnitude of Cr isotope fractionation associated with metamorphic processes. For this reason, we analyzed a set of subduction-related metamorphosed ultramafic rocks and fluid-altered carbonate rocks. The metamorphic age of these rocks range from Neoproterozoic to Phanerozoic. Although the pattern and depth of subduction may differ on the early and recent Earth, the underlying basic physicochemical processes (e.g., deformation,

100 temperature- or concentration-driven diffusion) are not likely to have varied over time.
101 Furthermore, the Cr isotopic composition of the mantle reservoir has been shown to be the same
102 within error since ~3.5 billion years ago (Ga) (Farkas et al., 2013). Therefore, Cr isotope behavior
103 during high temperature metamorphism derived from recent geological time should be applicable
104 to the Archean.

105

106 Third, our current understanding of the terrestrial Cr cycle is based largely on the study of
107 oxidative weathering of igneous rocks (Middelburg et al., 1988; Van der Weijden and van der
108 Weijden, 1995; Frei et al., 2009; Frei and Polat, 2012; Crowe et al., 2013). However, igneous rocks
109 represent only a small area of the subaerially exposed continental crust relative to sedimentary
110 rocks (e.g., Bluth and Kump, 1991). Therefore, weathering of sedimentary rocks can potentially
111 contribute significantly to riverine Cr flux to the ocean. Among sedimentary rocks, black shales are
112 of special interest because of their relatively high Cr concentrations. Given that black shale
113 weathering typically occurs at low pH, the framework developed from basalt weathering (e.g.,
114 Crowe et al., 2013; Berger and Frei, 2014; Frei et al., 2014) may not apply. Furthermore, previous
115 studies used lack of Cr isotope fractionation in sedimentary rocks to argue for low atmospheric
116 oxygen levels (e.g., Frei et al., 2009; Frei and Polat, 2012; Crowe et al., 2013; Planavsky et al., 2014).
117 However, absence of Cr isotope fractionation in sedimentary records is not necessarily a robust
118 evidence for absence of oxygen (Planavsky et al., 2014). This is because pyrite oxidation could
119 generate acids and dissolve solid Cr without Cr oxidation, and this process leads to Cr enrichment
120 but no isotope fractionation in sedimentary rocks (Konhauser et al., 2011). To resolve this
121 uncertainty, we targeted a well-studied black shale weathering profile to test whether there is Cr
122 isotope fractionation and Cr(III) oxidation in a high oxygen but low-pH weathering environment.

123

Lastly, interaction between seawater and oceanic crust is another process that can affect seawater $\delta^{53}Cr$ values. Although this process may not be very important on a global scale in the modern oceans (e.g., Reinhard et al., 2013), it may affect local water masses and sediments, given that large Cr isotope variations have been reported for Cr-rich hydrothermal minerals (Schoenberg et al., 2008; Farkas et al., 2013). Hydrothermal alteration may also have been important for global Cr isotope mass balance during the early periods of Earth's history due to higher heat flux and more mafic crust. It is essential to determine if there are significant Cr isotope fractionations in hydrothermal systems before using the Cr isotope composition of marine sediments to track surface oxidative processes. To further our understanding of seawater-oceanic crust interactions, we analyzed the Cr isotopic compositions of mildly altered oceanic crust and serpentinized peridotite samples from a range of localities.

2. Samples

We selected samples where geochemistry and geological context have been previously studied. Samples for metacarbonates, weathered black shales, altered oceanic crusts, serpentinites, Wudangshan basalts, and Dabie eclogites used powders from previous studies (references in Table 1). Below we provide only a short overview of the samples/sites and refer to previous work for more in-depth descriptions.

2.1. Basalts and eclogites

We examined basalt and eclogite samples from the ultra-high pressure Qinling-Tongbai-Dabie Orogenic Belt (QTDOB, Fig. 1). The QTDOB separates the North China Block (NCB) and South China Block (SCB), and itself is divided into the South Qinling (SQ) and North Qinling (NQ) orogens

by the Shangdan Fault. There were several major episodes of tectonic activity from mid-Proterozoic to Cenozoic time (e.g., Ratschbacher et al., 2003). The tholeiitic and alkaline basalt samples (~680–755 Ma) were sampled from the SQ, while the eclogite samples (~800 Ma) were sampled from the NQ. The basalts and eclogites are geographically close to each other and have the same source material (Ling et al., 2002; Wang et al., 2013). We examined the Cr isotope composition of tholeiitic and alkaline basalts because of their differing oxygen fugacities during formation (e.g., Carmichael and Ghiorso, 1986), which could potentially influence the redox geochemistry of Cr.

We also examined eclogite, metabasalt and metagabbro samples from Corsica, Greece, USA, and Norway—mafic rocks that experienced typical high pressure or ultrahigh-pressure metamorphism. Alpine Corsica (France) consists mainly of ophiolitic rocks and their sedimentary cover that underwent high-pressure blueschist–eclogite facies metamorphism during the Alpine orogeny Malavieille et al., 1998. One Corsican mafic pillow breccia (CRB) is from the Farinole-Volpajola eclogite unit that experienced metamorphism at ~520 °C and ~2.3 GPa (Vital Brovarone et al., 2011).

Blueschist–eclogite facies can be found in Syros and Tinos islands in Greece. The metamorphism was caused by subduction of the Apulian microplate beneath the Eurasia plate during the Eocene Alpine orogeny (Keiter et al., 2011 and references therein). Peak metamorphic conditions were ~500–550 °C and ~2.0 GPa (e.g., Trotet et al., 2001; Dragovic et al., 2012). Sample JAGSY-58A (37° 26.660’ N, 24° 53.327’ E) is an Mg-rich metagabbro from Kini Beach, Syros. It is dominated by large (cm-scale) bright green crystals of Cr-rich omphacite coexisting with phengite and chlorite. Sample JAGTI-1A is an eclogite from the Tinos subduction complex in the Kionia area (Broecker and Enders, 1999).

The USA Connecticut area experienced eclogite facies metamorphism during the collision of Laurentia with a Taconic arc complex ~456 Ma (Chu et al., in press). Sample JANW-17 is a retrograded eclogite from the Canaan Mountain Formation, northwestern Connecticut, USA (Harwood, 1979a; Harwood, 1979b). The eclogite facies assemblage consisted of omphacite, garnet, hornblende, phengite, epidote, and rutile; "peak" eclogite facies conditions were ~710 °C and 1.4–1.5 GPa (Chu et al., in press). Sample JAQ-158A is a hornblende cumulate ultramafic rock, consisting mostly of hornblende, orthopyroxene, olivine, phlogopite, aluminous spinel, and pyrrhotite. The hornblende is poikilitic and typically encloses orthopyroxene and olivine. These rocks are found as meter-scale pods and lenses within the ultrahigh-temperature (~1000 °C) gneisses of the Brimfield Schist in northeastern Connecticut, USA, described by Ague and Eckert (2012) and Ague et al. (2013).

The Franciscan Complex of California, USA, formed during eastward-directed subduction beneath the western margin of North America. The samples (CBJB2 and 6001) are from exotic blocks of metamorphosed mafic rock in the Central Belt mélange. Most metamorphic ages in the blocks range from Middle Jurassic to Early Cretaceous (see review in Wakabayashi, 1999). Sample 6001 is from the "Junction School eclogite" metamorphosed at maximum pressures of 1.8–2.2 GPa at ~550 °C (Page et al., 2007). The other Franciscan sample (CBJB2) is garnetiferous blueschist from Jenner Beach, which records metamorphic conditions of ~1.3 GPa and ~500 °C (Krogh et al., 1994).

193 Sample 4-1 is an ultrahigh-pressure kyanite eclogite from locality 1066 on Fjørtoft island,
194 Norway, metamorphosed at ultrahigh-pressures (UHP) near 4 GPa and temperatures of ~820 °C
195 (Terry et al., 2000). UHP conditions were reached when Baltica was subducted during the Scandian
196 orogeny (e.g., Carswell et al., 2006).

197

198 ***2.2. Metacarbonates***

199 Greenschist facies metacarbonate samples were taken from the Wepawaug Schist,
200 Connecticut, USA (see Ague, 2003 and references therein). We selected a transect (JAW-197) that
201 starts within a syn-metamorphic vein, through the reaction aureole, and into the wallrock (Fig. 2).
202 Infiltrating fluids precipitated albite, calcite, and quartz in the vein, and replaced muscovite with
203 albite in the reaction aureole. Fluid infiltration occurred under greenschist facies metamorphic
204 conditions (~425°C, 0.6–0.7 GPa) during the ~ 380 – 410 Ma Acadian orogeny (Lanzirotti and
205 Hanson, 1996; Ague, 2002; Lancaster et al., 2008). We focused on this transect given that previous
206 studies reported significant mass transfer of various elements including K, Na, Rb, Sr, Ba and REE,
207 indicating intense alteration at relatively high fluid-rock ratios (Ague, 2003).

208

209 ***2.3. Weathered black shale***

210 Weathered black shale samples were obtained from a road cut (37°52.167°N, 83°56.767°W)
211 near Clay City (Powell County, KY, USA) (Fig. 3). The road cut exposes a weathering profile through
212 the Upper Devonian (365 Myr) Ohio Shale, often referred to as the 'New Albany Shale' (NAS). The
213 samples were taken in 2000 (Jaffe et al., 2002) within a single stratigraphic horizon to avoid
214 syndepositional variation. The variations in the vertical position relative to the targeted
215 stratigraphic horizon are estimated to be less than 2 cm. The sample color ranged from brown near

the soil surface to black further into the weathering profile. Previous studies have found in the profile loss of organic carbon, pyrite S, mobile elements associated with reduced C/S phases such as Re and Os (Petsch et al., 2000; Petsch et al., 2001b; Jaffe et al., 2002) and disturbance to Re-Os isotope systems (Jaffe et al., 2002; Miller et al., 2015). The pH in the fluids from the shale profile could be as low as 1.8–2.1 (Sullivan et al., 1988; Jaffe et al., 2002). The outcrop is located south of the range of the late Cenozoic North American glaciation; therefore, weathering likely began before the onset of ice sheet growth. However, there are no robust estimates of the timescale of soil development.

2.4. Altered oceanic crust and serpentinites

We examined mildly hydrothermally altered oceanic crust samples derived from Ocean Drilling Program (ODP) Hole 504B (Fig. 4) spanning the upper ocean crust in the equatorial East Pacific (e.g., Alt et al., 1986; Bach et al., 2003). This is so far the deepest drill core into the oceanic crust and it has generated invaluable information on the petrology, geochemistry and physics of the upper oceanic crust over the past 20 years (Bach et al., 2003 and references therein). The basement section of the core (i.e., below 274.5 meter of sediments) can be divided into three zones (from top to bottom): a 571.5 meter Volcanic Zone (VZ) primarily consisting of pillowed and massive basalt flows; a 209 meter thick Transition Zone (TZ) with abundant dikes mixed with pillows and flows; and finally a >1045 meter Sheeted Dike Complex (SDC). There is a high percentage of brecciation in the TZ, and limited brecciation in other zones (~5%). Alteration is non-pervasive and is primarily concentrated in brecciated localities within the TZ. Samples included pillows (P), massive flows (M), breccias (B), and dikes (D). Samples with similar characteristics in each section were mixed in representative proportions in order to make composite samples (see Bach et al., 2003). Oxidative alteration is restricted to the uppermost 200–300 m of basement where the permeability is high,

240 with zoned oxidation halos commonly developed along clay/carbonate/oxyhydroxide grains (e.g.,
241 Alt et al., 1996). The alteration in the lower part of the VZ becomes non-oxidative and with
242 temperatures <150°C. Alteration temperature steeply increases to >250°C within the upper TZ and
243 then up to 500–600°C in the SDC.

244

245 Serpentinite samples examined in this study were obtained from the Iberian margin, Mid-
246 Atlantic Ridge (MAR) 15°20'N fracture zone, an ophiolite sequence in the Northern Apennines in
247 Italy, and a mélange from the Syros subduction complex. We investigated three drill cores from the
248 Iberian margin: Holes 897C and 897D from ODP Leg149 (see Sawyer et al., 1994), and Hole 1070A
249 from ODP Leg 173 (see Whitmarsh et al., 1998) (Fig. 5B). The peridotites from Site 897 are nearly
250 100% serpentinized with only minor olivine and pyroxene preserved. Serpentinization occurred at
251 low temperatures <150°C near the seafloor with high water/rock ratios and relatively high fO_2
252 coinciding with complete serpentinization and depletion of ferrous iron (Alt and Shanks, 1998).
253 Olivine and orthopyroxene are replaced by mesh- and bastite-textured serpentine and minor
254 magnetite. Two samples (897C-3 and 897C-7) were obtained from the 680–710 meter section of
255 Hole 897C and another two samples (897D-9 and 897D-13) were obtained from the 742–773 meter
256 section of Hole 897D (Fig. 5D). Three samples (1070A-1, 1070A-2, 1070A-3) were obtained from
257 the 705–707 meter section of Hole 1070A (Fig. 5E). In the sampled sections of Hole 1070A, between
258 95% and 100% of the primary minerals are replaced by serpentine, but with increasing depth
259 primary orthopyroxene and olivine can be sporadically found (Whitmarsh et al., 1998). Sampled
260 sections from Legs 149 and 173 have elevated sulfur concentrations and negative $\delta^{34}S$ values that
261 suggest extensive microbial reduction of seawater-sourced sulfate (Alt and Shanks, 1998;
262 Schwarzenbach et al., 2012). Late low-temperature fluid circulated through the upper part of the

serpentinite and resulted in the formation of abundant carbonate veins (Schwarzenbach et al., 2013).

Two drill cores were investigated from the MAR 15°20'N fracture zone: ODP Sites 1268A and 1272A (Fig. 5A). Two samples were obtained from each core: 1268A-1 and 1268A-2 in the 35–85 meter section, and 1272A-5 and 1272A-6 from the 99–108 meter section (Fig. 5C). The sampled interval of Hole 1272A comprises serpentinized harzburgite with minor dunite. The presence of iowaite in this section suggests fairly oxidizing conditions (Bach et al., 2004). The sampled interval of Hole 1268A comprises serpentinized and talc-altered harzburgite and dunite with pyrite veins (Paulick et al., 2006). At the same time, peridotites underwent two-stage alteration: initial serpentinization forming serpentine + magnetite ± pyrite, followed by talc replacing serpentine (Alt et al., 2007). The serpentinization temperatures are estimated to be <150°C and 250–350°C for 1270A and 1268A, respectively.

Three serpentinite samples (LA3a, LA20a, and LMO27) are from the Northern Apennine ophiolite in Italy (see Schwarzenbach et al., 2013). The ophiolite sequences exposed in this area are considered to result from the rifting of the European and Adriatic plates (~170 Ma) (more details in Schwarzenbach et al., 2013). Extensive calcite veins imply high water-rock ratios and oxidizing conditions with carbonate precipitation at <50–150°C and serpentinization temperatures <240°C (Schwarzenbach et al., 2013).

Three samples of ultramafic mélange matrix from the subduction complex exposed on Syros were also analyzed (JAGSY-8A-2, -12A, and -13C). Sample 8A-2 is rich in talc and chlorite and is

likely a physico-chemical admixture of ultramafic mélange matrix and metasomatised metamafic mélange block material (e.g., Marschall and Schumacher, 2012). Samples -12C and -13C are mantle-derived serpentinites from the mélange.

3. Methods

Samples provided as rock chips were crushed using a ceramic jaw crusher and then powdered with an agate mill. Powders (30 to 100 mg) were then digested with mixed HNO_3 and HF (3:1) on a hotplate. Fluorides were dissolved by repeated fluxing with 6 N HCl. Element concentrations were measured on a Thermo Scientific ElementXR ICP-MS. Prior to Cr purification via ion exchange methods, sample aliquots containing ~1 μg Cr were spiked with a ^{50}Cr-^{54}Cr double spike ($^{50}Cr/^{52}Cr$=462.917, $^{53}Cr/^{52}Cr$=0.580, $^{54}Cr/^{52}Cr$=354.450, calibrated in the Department of Geology, University of Illinois at Urbana-Champaign) so that the spike/sample ratio (i.e., $(^{54}Cr)_{spk}/(^{52}Cr)_{smp}$) was about 0.5.

For carbonate samples, we purified Cr following the methods described in Bonnand et al. (2011). This method utilizes the cation exchange resin AG50W-X8 (200–400 mesh) to separate Cr(III) cations from other matrix elements. For silicate samples we adopted procedures from Schoenberg et al. (2008), which utilize an anion exchange resin AG1-X8 (100–200 mesh) to separate Cr(VI) anions from matrix elements. For samples high in Fe, Ti, and V, further procedures are needed to remove these elements because they cause isobaric interferences. Residual Fe was separated from Cr in 6 N HCl by passing it through a micro column filled with 0.3 mL AG1-X8 (100-200 mesh) anion exchange resin; sample Cr was collected immediately after loading onto the column. Residual Ti and V were cleaned with a micro column filled with 0.3 mL AG 50W-X8 (200-

400 mesh) cation resin following previous methods (Trinquier et al., 2008). The yield for the Schoenberg et al. (2008) method combined with Fe and Ti removal procedures was typically higher than 80%. The yield for the Bonnand et al. (2011) method combined with Fe and Ti removal procedures were typically ~70%. These yields are acceptable since the ^{50}Cr-^{54}Cr double spike was added before column procedures and therefore, any isotope fractionation due to incomplete recovery is corrected. Procedural blanks were ~0.7 ng and ~20 ng for the cation exchange and anion exchange methods, respectively. The relatively high blank for the anion exchange method was due to the use of the oxidant ammonium persulfate [Acros (99+%) and Sigma Aldrich (≥98%)]. Sample to blank signal ratios range from 1400:1 to 50:1 and blank $\delta^{53}Cr$ was measured to be 0.0±0.2‰. Therefore, blank correction was not performed.

Chromium isotopic compositions were measured on a Neptune Plus MC-ICP-MS housed in the Yale Metal Geochemistry Center in the Department of Geology & Geophysics. Purified Cr samples dissolved in 0.7 N HNO_3 with concentrations of ~250 µg/g were introduced to the plasma with a PFA µFlow nebulizer (~50 µL/min) coupled with an Apex IR desolvating introduction system (Elemental Scientific) without additional gas or membrane desolvation. With a standard sample cone and X skimmer cone and under high-resolution mode, the obtained sensitivity was ~3×10^{-10} A ^{52}Cr on 1 µg/g Cr solution. All ion beams were measured on faraday detectors. The isotopes ^{49}Ti, ^{51}V, and ^{56}Fe were measured to monitor and correct for isobaric interferences of ^{50}Ti, ^{50}V, and ^{54}Fe. The unprocessed NIST SRM 979 standard was analyzed after every three samples to monitor instrument drift, which was <0.1‰ (Fig. 6). Sample $\delta^{53}Cr$ values were normalized to the average value of the bracketing NIST SRM 979. The NIST SRM 3112a and geostandard BHVO-2 (USGS) were also treated as samples through the digestion and ion exchange procedures and yielded $\delta^{53}Cr$ values of -0.01±0.08‰ (2SD, n=10) and -0.11±0.08‰ (2SD, n=7), respectively (Table

S1), after normalization to NIST SRM 979. These values agree well with previously reported values (Schoenberg et al., 2008). Therefore, we used 0.08‰ as the external reproducibility for samples.

4. Results

Results for all samples are provided in Table 1 and below we describe each sample groups separately.

4.1. Basalts and eclogites

Over a wide range of Cr concentrations (Fig 7.), the examined basalts and eclogites yielded δ^{53}Cr values within a narrow range, -0.12±0.13‰ (2SD, n=33). There was no analytically resolvable difference in δ^{53}Cr values between alkaline basalt, tholeiitic basalt, metabasalt, metagabbro, and eclogite samples.

4.2. Metacarbonates

Values for Cr/Zr (Zr serving as a relatively immobile element for normalization purposes) showed a decreasing trend from the relatively fresh wallrock to the vein-wallrock boundary. This matches well with the trend observed in K/Zr (Fig. 8), suggesting loss of elements during fluid-rock interaction. The Cr/Zr ratios in the unaltered portion of the traverse lie slightly above the value estimated for the upper continental crust (Rudnick and Gao, 2003), but decrease to below this value approaching the vein. The metacarbonate rocks were pulverized in agate only, without contact with ceramic material. Therefore, the use of Zr as the normalization element is valid. Despite the

significant mobility of Cr evidently caused by the vein-forming fluid, the $\delta^{53}Cr$ values along the transect are all within analytical of one another.

4.3. Black shale weathering

We observed enrichment of Cr and high $\delta^{53}Cr$ values in the most altered portions of the NAS black shale weathering profile (Fig. 9). The Cr/Ti ratios throughout the weathering profile range from 0.015 to 0.021, which overlap with the ranges reported for the upper continental crust (0.0158 to 0.0240, Condie, 1993; McLennan, 2001; Rudnick and Gao, 2003). However, the Cr/Ti ratios in the most weathered section are about 30% higher than the pristine shale and the $\delta^{53}Cr$ value is 0.5‰ heavier. The enrichment of Cr in the surface sample is in sharp contrast to depletion of organic matter and the mobile element rhenium. Deeper samples in the profile have $\delta^{53}Cr$ values that are similar to or slightly higher than that in the pristine shale, except for one sample (NAS-20), which yielded a $\delta^{53}Cr$ value of -0.5‰.

4.4. Altered oceanic crust and serpentinites

Samples from ODP Hole 504B yielded $\delta^{53}Cr$ values (Table 1; Fig. 11) that ranged between -0.22‰ and -0.17‰, with an average of -0.18±0.10‰ (2SD, n=7), which is within the previously reported range for bulk silicate earth (BSE) (Schoenberg et al., 2008; Moynier et al., 2011; Farkas et al., 2013) and identical to the measured basalts reported above. Chromium concentrations range from 199 μg/g to 387 μg/g. No systematic trends were observed in $\delta^{53}Cr$ values between different alteration zones. However, Cr concentrations tend to be lower in the brecciated zone, where alteration is most intensive.

In contrast, the examined serpentinite samples had a range of $\delta^{53}Cr$ values of -0.18‰ to 0.52‰ and concentrations varied from 595 μg/g to 3038 μg/g (Fig. 12). Samples with lower Cr concentrations tend to have larger $\delta^{53}Cr$ values. Further, Cr concentrations in most of the altered peridotites are markedly lower than the estimated average mantle value of 2625 μg/g (blue line in Fig. 12; Sun and McDonough, 1989), indicating loss of Cr during serpentinization.

5. Discussion

5.1. Basalts and eclogites

The $\delta^{53}Cr$ values of the investigated basalt and eclogite samples fall within previously reported ranges of the BSE (Schoenberg et al., 2008; Farkas et al., 2013; Shen et al., 2015) (Fig. 7). Based on high temperature rocks/minerals published so far (Schoenberg et al., 2008; Farkas et al., 2013; Shen et al., 2015; this study), the average $\delta^{53}Cr$ values for fresh silicate rocks (43 samples), metamorphosed silicate rocks (50 samples), and mantle chromites (39 samples) are -0.13±0.13‰, -0.11±0.13‰, and -0.07±0.13‰, respectively (Table S2). All three groups are within error the same, suggesting that there is very limited Cr isotope fractionation under high temperature conditions. Although the number of high temperature samples has nearly tripled, the original BSE value of -0.124±0.101‰, proposed by Schoenberg et al. (2008) is still valid.

The BSE value can be compared with the value for bulk Earth (BE) as inferred from analyses of carbonaceous chondrites. Moynier et al. (2011) reported an average value of -0.32±0.05‰ from carbonaceous chondrites, which is significantly lower than the BSE range. However, more recent

measurements on a limited number of carbonaceous chondrites did not find supporting evidence for significantly lower BE values (Qin et al., 2015). The discrepancy between Moynier et al. (2011) and Qin et al. (2015) may imply that there is Cr isotope heterogeneity in carbonaceous chondrites; additional measurements are needed to test this idea. Nevertheless, given the lower-than-BSE values observed by Moynier et al. (2011), the authors suggested that Earth's core-mantle differentiation induced significant Cr isotope fractionation with light isotopes being incorporated into the core. However, significant equilibrium Cr isotopic fractionation is not likely under high temperatures, as predicted by *ab initio* calculations (Moynier et al., 2011) and natural observation of a wide range of high-temperature rocks (Schoenberg et al., 2008; Farkas et al., 2013; Shen et al., 2015; this study). Therefore, the apparent difference in δ^{53}Cr values between the BSE and BE, if true, suggests that either core-mantle differentiation on Earth occurred under relatively low temperature conditions (e.g., during early accretion, Moynier et al., 2011) or that some kinetic process (e.g., thermal diffusion, Furry et al., 1939; Richter et al., 2008; Huang et al., 2010) may have induced Cr isotope fractionation under conditions of higher temperature and pressure. Further analysis of a range of solar system materials can be leveraged to test these alternate hypotheses.

5.2. Metacarbonates

Despite significant element mobility during alteration of the Wepawaug Schist sample, there appears to be no significant effect on the Cr isotope composition (Fig. 8). As muscovite was almost certainly the major Cr host in the metacarbonate rock, the metasomatic destruction of this phase led to the observed losses of Cr and K (Ague, 2003). The δ^{53}Cr values near and within the reaction aureole are slightly lower than the more distal samples by ~0.04‰, and the trend appears to be systematic, but the variation is well within the analytical uncertainty. This lack of significant variation in δ^{53}Cr values suggests that rocks that have experienced significant metamorphic

alteration at relatively high fluid-rock ratios may still record primary Cr isotope signatures, as long as there is no enrichment of Cr from isotopically distinct sources. However, the presence of organic matter and pyrite (Fig. 2) in the Wepawaug Schist carbonate rock indicates overall low fO_2. Oxidizing metamorphic conditions should be tested in the future for potentially pronounced Cr isotope effects.

5.3. Black shale weathering

There is significant enrichment of Cr and large variation (up to 1‰) in Cr isotopic composition in the New Albany Shale weathering profile (Fig. 9). The positive $\delta^{53}Cr$ values in all but one sample (NAS20) and the enrichment of Cr at the profile surface is in sharp contrast to those observed in basaltic weathering profiles (Frei and Polat, 2012; Crowe et al., 2013; Frei et al., 2014), where Cr depletion and negative isotope fractionation were observed. We propose that the Cr enrichment on the surface of the shale profile is due to short transport followed by immobilization of isotopically heavy Cr(VI). The immobilization could be caused by quantitative reduction or adsorption. Reduction is possible given the elevated remaining organic carbon content (~2 wt.%) despite significant loss relative to the less weathered interior portion of the outcrop (6–8%). However, the remaining organic is unlikely to be labile and active enough to reduce Cr(VI) (e.g., Petsch et al., 2001b). Alternatively, given the high Fe oxide concentrations (likely formed during initial organic carbon loss) near the surface (Fig. 9E), adsorption of Cr(VI) to Fe oxides or trapping of Cr(VI) during oxide precipitation (co-precipitation) may also have lead to the enrichment of Cr on the surface. Indeed, there is a positive correlation between Cr/Ti ratios and Fe concentrations (Fig. 10). We emphasize that the observed behavior of Cr isotopes in this profile differs from that of Re isotopes in that mobile heavy Re is not immobilized near the soil surface, but instead lost from the profile (Miller et al., 2015).

The single sample with a negative $\delta^{53}Cr$ (-0.52‰) also has two possible explanations. First, this sample is found close to the redox front within the weathering transect (e.g., Jaffe et al., 2002), and it is possible that this sample locality was undergoing active redox reaction and influenced by local partial Cr reduction during weathering that is not yet apparent in, for example, organic carbon content. Therefore, this sample may simply have captured the partially reduced, isotopically light Cr(III). The Re content in the same sample is enriched relative to adjacent samples, which is consistent with reductive sequestration of redox-sensitive elements at this particular locality. However, by mass balance, significant Cr enrichment would have been required to result in such a negative $\delta^{53}Cr$ value, and such enrichment is not observed for this sample and is thus unlikely. Alternatively, the negative $\delta^{53}Cr$ value may be due to loss of heavy Cr during isotope exchange between solid Cr(III) and soluble Cr(VI) carried by weathering fluids (e.g., Wang et al., 2015a). This isotope exchange process is able to generate large isotope fractionation without net changes in Cr enrichment.

In any case, the relatively large range of $\delta^{53}Cr$ values (up to 1‰) in the NAS weathering profile provides clear evidence that there can be active Cr redox cycling in low pH oxidative weathering environments. Manganese oxides are so far the only oxidants found to induce significant Cr(III) oxidation in natural environments (e.g. Eary and Rai, 1987). Formation of manganese oxides is primarily mediated by microorganisms (Tebo et al., 2004) whose growth has been generally deemed to be hindered under low pH conditions (e.g., Mayanna et al., 2015) such as those found in black shale weathering environments (Sullivan et al., 1988; Jaffe et al., 2002). However, some studies have reported microorganisms that can thrive under acidic conditions

(Petsch et al., 2001a) and generate manganese oxides (Mayanna et al., 2015). This is in line with our observation of relatively large Cr isotope fractionations in an acidic shale weathering environment.

The examined profile is only a single system, but it provides support for the notion that a lack of Cr isotope variation in sedimentary records (e.g., as captured in pre-Great Oxidation Event and mid-Proterozoic sedimentary rocks) cannot be well explained by oxidative weathering of a poorly buffered shale-dominated catchment. Instead, it is more likely linked to low oxygen levels at Earth's surface (e.g., Frei et al., 2009; Planavsky et al., 2014). However, this inference rests on the assumption that weathering of black shales is a significant source of Cr to rivers and thus oceans. Given the Cr enrichment in the outer portions of the weathering profile, an intriguing alternative possibility is that weathering of organic-rich shale may not contribute significant Cr fluxes into rivers, and may instead serve as a 'trap' of Cr that is ^{53}Cr-enriched. In this scenario, our finding of significant Cr isotope fractionation during black shale weathering may not be relevant to Precambrian cycling of mobile, unfractionated Cr. More studies of the behavior of redox-sensitive isotope systems (e.g. Cr, Mo, Re, U) in organic-rich shale weathering profiles coupled to surface water analyses should be conducted in the future in order to better constrain contributions to global mass balance from weathering sedimentary rocks relative to weathering of igneous rocks.

5.4. Hydrothermal alteration

The majority of the analyzed serpentinites (Fig. 12) show elevated δ^{53}Cr values (up to ~0.5‰) compared to fresh peridotite (-0.10‰ to -0.21‰; Schoenberg et al., 2008). The values fall within previously reported values for serpentinites (-0.17‰ to ~1.2‰, Farkas et al., 2013). Two processes may be responsible for producing the positive δ^{53}Cr values: (1) incorporation of

492 isotopically heavy Cr from seawater; and (2) loss of isotopically light Cr from peridotite during
493 hydration processes.

494

495 A simple two-end-member mass balance calculation indicates that direct addition of
496 seawater Cr to fresh peridotite is not likely to induce such large isotope shifts. We assume that: (1)
497 Seawater (0.2 ng/g Cr, Jeandel and Minster, 1987) circulates through the upper oceanic crust (2625
498 μg/g Cr, Sun and McDonough, 1989; 1000 m thick with a density of 2700 kg/m^3, Staudigel, 2014;
499 area of 2.97×10^8 km^2, Parsons, 1981) with a water flux of about 6.4×10^{14} kg/yr (Staudigel, 2014)
500 for 100 million years; (2) Cr from seawater gets evenly added to the upper oceanic crust; and (3) Cr
501 in seawater is completely sequestered. Given these assumptions, which are conservative with
502 respect to both water flux and sealing time for the oceanic crust, we find that the amount of Cr
503 supplied by seawater within the 100 million-year alteration timeframe is about six orders of
504 magnitude lower than the size of the native Cr reservoir of the upper oceanic crust. Thus, the
505 isotope effect on the upper oceanic crust as a whole should be negligible. However, we acknowledge
506 that this simple calculation does not rule out localized Cr enrichments. Nevertheless, it is much
507 more likely that isotope variations in serpentinites originate from redox cycling within the upper
508 oceanic crust, rather than addition of Cr directly from seawater.

509

510 Loss of isotopically light Cr during the hydration processes is a possible explanation for the
511 enrichment of heavy Cr during serpentinization. However, previous experimental (Zink et al., 2010)
512 and field (Frei and Polat, 2012; Crowe et al., 2013) observations found that heavy isotopes are
513 preferentially lost during Cr oxidation. Importantly, measurements on crocoite ($PbCrO_4$), which is
514 thought to precipitate directly from oxic hydrothermal fluids, yielded heavy δ^{53}Cr values ranging
515 from 0.01‰ to 1.96‰ (Schoenberg et al., 2008; Farkas et al., 2013). This direction of isotope

fractionation during oxidation of Cr(III) is opposite to the prediction by mass-dependent kinetic isotope effect, whereby light isotopes tend to react 'faster' and thus enrich in the product (e.g. Bigeleisen, 1965), but is consistent with the prediction by equilibrium isotope effect, whereby heavier isotopes preferentially enrich in species with stronger chemical bonds, i.e. CrO_4^{2-} (Schauble et al., 2004; Wang et al., 2015a). However, the fractionation during oxidation is still poorly constrained, and likely depends on the oxidation kinetics. Further, there is some evidence of isotopically light Cr(VI) generated by oxidation (Bain and Bullen, 2005), possibly due to a kinetic isotope effect. Therefore, we can estimate the size of the oxidation fractionation assuming all Cr loss from peridotite to fluids is due to oxidation. We get a fractionation factor ($\varepsilon_{fluid\text{-}peridotite}$) of -0.6‰ to -0.17‰ (Fig. 12), using a Rayleigh fractionation model:

$$\delta^{53}Cr = [\delta^{53}Cr_{initial} + 10^3]f^{(\alpha-1)} - 10^3,$$

where $\delta^{53}Cr_{initial}$ is the δ^{53}Cr value of peridotites and a value of -0.2‰ is used (the lowest of the examined serpentinites); f is the fraction of Cr remaining after serpentinization, calculated as $[Cr]_{serpentinite}$ divided by the mantle value (2625 μg/g Cr); α is the fractionation factor and can be converted to $\varepsilon_{fluid\text{-}peridotite}$ by the equation:

$$1000(\alpha-1) \approx \varepsilon_{fluid\text{-}peridotite}.$$

An alternative mechanism for generating isotopically heavy serpentinite is through multi-stage alteration. The Cr concentrations in the examined serpentinites are up to about four times

lower than the average mantle value (2625 μg/g, Sun and McDonough, 1989). This suggests that the peridotites experienced net Cr loss. The loss of Cr is likely through oxidative mobilization of Cr(III) in peridotite instead of direct dissolution, given the extremely low solubility of Cr(III) (Rai et al., 1987) under the high pH (9–9.8) conditions generated by serpentinization (Kelley et al., 2001; Kelley et al., 2005). However, serpentinization generally proceeds under reducing conditions in the early stages (e.g., Berndt et al., 1996; Seyfried et al., 2007), usually at high temperatures, followed by oxidizing conditions during later stages (e.g., Alt and Shanks, 1998), usually at low temperatures. Therefore, the loss of Cr likely occurred during later stages of serpentinization. The Cr isotope fractionation during oxidation of solid-state Cr(III) is not been well understood, but we expect it to be small due to a "rind effect" that has been reported for oxidation of solid-phase U(IV) by dissolved oxygen (see Wang et al., 2015b). Further, the long timescales of hydrothermal circulation ($\sim 10^6$ years) may allow isotope equilibration between Cr(III)-bearing residual peridotite and Cr(VI)-bearing serpentinization fluid. However, such isotope equilibration should lead to isotopically light Cr(III) phase (Schauble, 2007; Wang et al., 2015a), unless the amount of Cr(VI) in the fluid dominates the Cr contained in the serpentinized peridotites and is very enriched in ^{53}Cr ($\delta^{53}Cr$ >5.8‰). Therefore, it is possible that the high $\delta^{53}Cr$ values in the serpentinized peridotites could alternatively be caused by addition of isotopically heavy Cr from alteration fluids after the peridotite had lost the majority of their original Cr. Fluids carrying the oxidized Cr(VI) may experience partial reduction during migration, leading to isotopically heavy residual Cr(VI) in the fluid. This isotopically heavy Cr(VI) can be added to the Cr-depleted serpentinites via reduction. By mass balance, $\delta^{53}Cr$ values of serpentinites that have lost the majority of their Cr can be relatively easily altered by addition of isotopically heavy Cr from fluids.

Such a multi-stage redox alteration model as outlined above is consistent with sulfur isotope data from the serpentinite samples obtained from Legs 149 and 173 (Alt and Shanks, 1998; Schwarzenbach et al., 2012). Both sulfide and sulfate concentrations (Fig. 13D) in these samples are much higher than the average total S in the mantle (McDonough and Sun, 1995). Furthermore, the $\delta^{34}S$ values for both sulfide and sulfate in the serpentinites (Fig. 13C) are lower than the seawater and mantle value (see Alt and Shanks, 1998). These observations suggest significant addition of isotopically light sulfur (Fig. 13C) through sulfate reduction. Such reducing conditions may have enabled quantitative reduction of isotopically heavy Cr(VI) carried by the fluids. Furthermore, transport of sulfate supports that oxic conditions existed in the system to allow loss of Cr from peridotites. However, to satisfy isotope mass balance there must be isotopically light Cr produced by partial reduction when the fluid migrates within the upper oceanic crust. As the fluid migrates, the partially reduced, isotopically light Cr may have been diluted into less altered samples with roughly BSE $\delta^{53}Cr$ values with high Cr concentration, and thus making the isotope shift muted. Alternatively, our sampling may have missed a zone of the serpentinizing system with light $\delta^{53}Cr$ values.

In any case, large isotope fractionations in serpentinizing systems are significant given that small Cr isotope variations in sedimentary rocks proximal to hydrothermal systems have been used to track the emergence of biological oxygen production. This and other recent work (Farkas et al., 2013) indicates that a hydrothermal origin of Cr must be ruled out before fractionated Cr in the sedimentary record can be linked unambiguously with terrestrial Cr redox cycling. Although we expect that from a mass balance perspective the overall effect of serpentinizing systems on the Earth surficial Cr isotope cycle is likely to be small on a global scale, the possibility for strongly

584 fractionated high-temperature Cr sources in restricted basins or regions should be kept in mind in
585 future studies (e.g., Farkas et al., 2013).

586

587 **6. Concluding marks**

588 Basalts and their metamorphic products yielded similar $\delta^{53}Cr$ values to published values of
589 silicates and chromites. This suggests limited Cr isotope fractionation under high temperature
590 conditions. Furthermore, carbonate rocks that have experienced significant fluid infiltration during
591 regional metamorphism show very limited Cr isotope fractionation. These results suggest that
592 sedimentary and igneous Cr isotope signatures may not to be strongly altered by metamorphic
593 alteration, as long as there is minimal transport of isotopically distinct Cr to/from the system and
594 there is no significant shift in redox state.

595

596 Up to ~1‰ variation in $\delta^{53}Cr$ values in a black shale weathering profile are suggestive of
597 active redox cycling of Cr driven by manganese oxide formation in an acidic black shale weathering
598 environment. However, net isotope variation may be restricted for the shale weathering profile as a
599 whole due to efficient short-range immobilization of the oxidized Cr(VI).

600

601 Mild alteration of mafic oceanic basalt by seawater does not appear to fractionate Cr
602 isotopes significantly. However, serpentinization of ultramafic peridotites results in serpentinites
603 with large positive $\delta^{53}Cr$ values. These high $\delta^{53}Cr$ values can be explained by a kinetic isotope
604 fractionation during loss of Cr during serpentinization, or by a multistage alteration hypothesis
605 where peridotites lose Cr via oxidation without significant isotope fractionation in the first stage

and then accumulates isotopically heavy Cr through later-stage sulfate reduction. Significant Cr isotope fractionation during serpentinization indicates that a hydrothermal origin of Cr must be ruled out before fractioned Cr in the early sedimentary record can be linked robustly to terrestrial Cr redox cycling.

Acknowledgement

Funding for this research was provided by Agouron Institute to XLW, National Science Foundation (NSF) EAR-0105927 and EAR-1250269 to JJA, and NSF EAR-1324566 to ES. NJP and CTR acknowledge funding from the Alternative Earths NAI. XLW wishes to thank T.M. Johnson for providing the chromium double spike, Wen-Li Ling for providing Wudangshan basalt samples and Ci Zhang for logistic handling of the Qinling-Tongbai-Dabie samples. JJA thanks E.F. Baxter, O. Beyssac, M.T. Brandon, C.M. Breeding, M. Broecker, X. Chu, and A. Vitale Brovarone for samples and discussions, and the Deep Carbon Observatory, and Yale University for support. This research used samples provided by the Ocean Drilling Program (ODP). The authors would like to thank Dr. Catherine Chauvel for handling the manuscript and three anonymous reviewers for providing constructive comments that greatly improved the quality of the original manuscript.

Figure captions

Figure 1. A tectonic sketch of the Qinling-Tongbai-Dabie orogen separating the north China block from the south China block. Basalt samples are from South Qinling and eclogite samples are from North Qinling. Detailed geological setting information can be found in Wang et al. (2013) and Ling et al. (2002).

Figure 2. Images for the metacarbonate rock from the Wepawaug Schist. A: A photograph showing the vein intruding the wall rock, generating a reaction aureole. Cal, Ank, Qtz, Ab, Chl, Rt, Ms refer to calcite, ankerite, quartz, albite, chlorite, rutile, and muscovite, respectively. The fluid was associated with regional metamorphism (~380–410 Ma) during the Acadian orogeny that created the Wepawaug Schist, Connecticut, USA. Details on the geological setting are provided in Ague (2003). The dashed line shows the sampled transect with distance being zero in the center of the vein and increasing toward the right side of the image. B: Mineral assemblage of the vein. Note the calcite rims surrounding the albite grains. C: The contact between the reaction aureole and the vein. Note the pyrite within the aureole. D: Organic matter within the aureole. E: Wallrock with no apparent alteration. F: Albite and chlorite near the contact.

Figure 3. A schematic of the New Albany Shale weathering profile exposed by a road cut near Clay City, Kentucky, USA. The light gray layer represents weathered black shale whereas the darker gray represents deeper layers that are relatively unweathered. Circles represent sampling points. Care was taken to sample from the same horizon to avoid potential syn-depositional variations. Further information can be found in Jaffe et al. (2002).

Figure 4. Location of ODP Hole 504B in the Equatorial Eastern Pacific. On the left is the simplified lithological column in meters below basement (mbbm). Depth in meters below seafloor is also indicated. The basement rock is divided into a volcanic zone, transition zone, and sheeted dike zone. Brecciation is developed in each zone and occurs where alteration is most intensive. Samples with similar characteristics in each section are combined in representative proportions in order to create composite samples. Further information is given in Bach et al. (2004).

Figure 5. Locations of ODP drill cores from the Iberia margin and the 15°20'N Mid-Atlantic-Ridge Fracture Zone, and simplified lithological columns of all the cores from which the investigated serpentinite samples were obtained. Red stars denote sample localities; numbers next to the red stars are $\delta^{53}Cr$ values (±0.08‰). Further information for the cores can be found in Sawyer et al. (1994), Whitmarsh et al., 1998, and Shipboard Scientific Party (2004).

Figure 6. Reproducibility of SRM 979 standard analyzed during this study (-0.08±0.05‰, 2SD, n=64). The dashed lines represent the 2SD envelope. Samples are normalized to the average $\delta^{53}Cr$ value of SRM 979 of each session, during which the SRM 979 $\delta^{53}Cr$ variation is typically less than 0.1‰.

Figure 7. $\delta^{53}Cr$ values of high temperature igneous rocks and their metamorphosed equivalents, plotted against their Cr concentrations. The average $\delta^{53}Cr$ for fresh silicates (n=43), metamorphosed silicates (n=50), and chromites (n=39) are -0.13±0.13‰ (2SD), -0.11±0.13‰ (2SD), and -0.07±0.13‰ (2SD), respectively (data compiled in Table S1). Note that the x-axis is on logarithmic scale.

Figure 8. $\delta^{53}Cr$ values, Cr/Zr ratios, and K_2O/Zr ratios for the metacarbonate rock from Wepawaug Schist. The red bar in B indicates upper continental crust Cr/Zr ratio. Yellow shaded region denotes the vein and gray shaded region denotes the reaction aureole. The error bars are the external analytical uncertainty (0.08‰, see 'Methods' section).

675

676 Figure 9. $\delta^{53}Cr$ values, Cr/Ti ratios, organic carbon, Re/Ti ratios, and Fe concentration for the New
677 Albany Shale weathering profile. Data other than $\delta^{53}Cr$ and Cr/Ti ratios are from Jaffe et al. (2002).
678 The shaded area in A represents the estimated BSE range (Schoenberg et al., 2008 and Farkas et al.,
679 2013; this study); the shaded area in B represents estimated upper continental crust Cr/Ti (Condie,
680 1993; McLennan, 2001; Rudnick and Gao, 2003). The vertical dashed line shows the boundary of
681 visible weathering.

682

683 Figure 10. Cr/Ti ratios plotted as a function of iron content. The positive correlation suggests that
684 the Cr enrichment on the surface of the NAS weathering profile is a result of adsorption of mobile
685 Cr(VI) to the iron oxides.

686

687 Figure 11. $\delta^{53}Cr$ values and Cr concentrations for altered oceanic crust composite samples from
688 ODP drill core 504B. The blue shaded region in A denotes the 2SD range around the average $\delta^{53}Cr$
689 value of the basalt flows and fresh sheeted dike samples, which we use to represent the least
690 altered oceanic crust; the blue shaded region in B represents the average Cr concentration of the
691 same samples. Note that the samples are composite samples and therefore the plotted depth does
692 not represent true depth.

693

694 Figure 12. $\delta^{53}Cr$ values plotted against Cr concentration for the serpentinite samples examined in
695 this study. The horizontal gray bar denotes $\delta^{53}Cr$ range for the North Atlantic seawater (Scheiderich
696 et al., 2015); the vertical gray bar denotes the estimated Cr concentration of the mantle (Sun and
697 McDonough, 1989), which is thought to represent average fresh peridotites. Altered peridotites
698 with heavy $\delta^{53}Cr$ values have less Cr than average fresh peridotite, suggesting that the heavy $\delta^{53}Cr$
699 values are not a result of direct addition of seawater Cr. The high $\delta^{53}Cr$ values are possibly due to
700 kinetic isotope fractionation where light isotopes were preferentially lost. The dashed trends are
701 modeled using a Rayleigh fractionation model. The fractionation factors used are -0.6‰ and -
702 0.17‰. The initial $\delta^{53}Cr$ value used is -0.2‰.

703

704 Figure 13. $\delta^{53}Cr$ values, Cr concentrations, $\delta^{34}S$ values, and sulfur concentrations in the examined
705 serpentinites. The gray and blue bars in A denote $\delta^{53}Cr$ range for the BSE (Schoenberg et al., 2008
706 and Farkas et al., 2013; this study) and the North Atlantic seawater (Scheiderich et al., 2015),
707 respectively. The blue bar in B denotes mantle Cr concentration estimates (Sun and McDonough,
708 1989). Sulfur data are from Alt and Shanks (1998) and Schwarzenbach et al. (2012). Dashed and
709 solid blue lines in C indicate $\delta^{34}S$ values for the mantle and modern seawater, respectively (Alt and
710 Shanks, 1998). Blue dashed line in D shows the sulfur concentration of the mantle (McDonough and
711 Sun, 1995).

712

713 **References**

714 Ague, J.J., 2002. Gradients in fluid composition across metacarbonate layers of the Wepawaug
715 Schist, Connecticut, USA. Contributions to Mineralogy and Petrology, 143(1): 38-55.

716 Ague, J.J., 2003. Fluid infiltration and transport of major, minor, and trace elements during regional
717 metamorphism of carbonate rocks, Wepawaug Schist, Connecticut, USA. American Journal
718 of Science, 303(9): 753-816.

719 Ague, J.J., Eckert, J.O., 2012. Precipitation of rutile and ilmenite needles in garnet: Implications for
720 extreme metamorphic conditions in the Acadian Orogen, USA. American Mineralogist, 97(5-
721 6): 840-855.

722 Ague, J.J., Eckert, J.O., Chu, X., Baxter, E.F., Chamberlain, C.P., 2013. Discovery of ultrahigh-
723 temperature metamorphism in the Acadian orogen, Connecticut, USA. Geology, 41(2): 271-
724 274.

725 Alt, J.C., Honnorez, J., Laverne, C., Emmermann, R., 1986. Hydrothermal alteration of a 1 km section
726 through the upper oceanic crust, Deep Sea Drilling Project Hole 504B: Mineralogy,
727 chemistry and evolution of seawater‐basalt interactions. Journal of Geophysical Research:
728 Solid Earth (1978–2012), 91(B10): 10309-10335.

729 Alt, J.C., Shanks, W.C., 1998. Sulfur in serpentinized oceanic peridotites: Serpentinization processes
730 and microbial sulfate reduction. Journal of Geophysical Research: Solid Earth (1978–2012),
731 103(B5): 9917-9929.

732 Alt, J.C. et al., 2007. Hydrothermal alteration and microbial sulfate reduction in peridotite and
733 gabbro exposed by detachment faulting at the Mid‐Atlantic Ridge, 15° 20′ N (ODP Leg
734 209): A sulfur and oxygen isotope study. Geochemistry, Geophysics, Geosystems, 8: Q08002,
735 doi:10.1029/2007GC001617.

736 Alt, J.C. et al., 1996. Ridge-flank alteration of upper ocean crust in the eastern Pacific: Synthesis of
737 results for volcanic rocks of Holes 504B and 896A. In: Alt, J.C., Kinoshita, H., Stokking, L.B.
738 (Eds.), Proceedings of the Ocean Drilling Program, Scientific Results, College Station, TX
739 (Ocean Drilling Program), vol. 148, pp. 435-452.

740 Bach, W., Garrido, C.J., Paulick, H., Harvey, J., Rosner, M., 2004. Seawater‐peridotite interactions:
741 First insights from ODP Leg 209, MAR 15 N. Geochemistry, Geophysics, Geosystems, 5:
742 Q09F26, doi:10.1029/2004GC000744.

743 Bach, W., Peucker-Ehrenbrink, B., Hart, S.R., Blusztajn, J.S., 2003. Geochemistry of hydrothermally
744 altered oceanic crust: DSDP/ODP Hole 504B-Implications for seawater-crust exchange
745 budgets and Sr and Pb isotopic evolution of the mantle. Geochemistry, Geophysics,
746 Geosystems, 4: 8904, doi:10.1029/2002GC000419.

747 Bain, D.J., Bullen, T.D., 2005. Chromium isotope fractionation during oxidation of Cr (III) by
748 manganese oxides. Geochimica et Cosmochimica Acta, 69: S212.

749 Berger, A., Frei, R., 2014. The fate of chromium during tropical weathering: A laterite profile from
750 Central Madagascar. Geoderma, 213: 521-532.

751 Berndt, M.E., Allen, D.E., Seyfried, W.E., 1996. Reduction of CO2 during serpentinization of olivine at
752 300 C and 500 bar. Geology, 24(4): 351-354.

753 Bigeleisen, J., 1965. Chemistry of isotopes. Science, 147(3657): 463.

754 Birck, J.L., Allègre, C.J., 1984. Chromium isotopic anomalies in Allende refractory inclusions.
755 Geophysical Research Letters, 11(10): 943-946.

756 Bluth, G.J., Kump, L.R., 1991. Phanerozoic paleogeology. Am. J. Sci, 291(3): 284-308.

757 Bonnand, P., Parkinson, I.J., James, R.H., Karjalainen, A.-M., Fehr, M.A., 2011. Accurate and precise
758 determination of stable Cr isotope compositions in carbonates by double spike MC-ICP-MS.
759 Journal of Analytical Atomic Spectrometry, 26(3): 528-535.

760 Broecker, M., Enders, M., 1999. U–Pb zircon geochronology of unusual eclogite-facies rocks from
761 Syros and Tinos (Cyclades, Greece). Geological Magazine, 136(02): 111-118.

762 Carmichael, I.S., Ghiorso, M.S., 1986. Oxidation-reduction relations in basic magma: a case for
763 homogeneous equilibria. Earth and Planetary Science Letters, 78(2): 200-210.

764 Carswell, D., Van Roermund, H., de Vries, D.W., 2006. Scandian ultrahigh-pressure metamorphism of
765 proterozoic basement rocks on Fjørtoft and Otrøy, Western Gneiss Region, Norway.
766 International Geology Review, 48(11): 957-977.

767 Chu, X., Ague, J.J., Axler, J.A., Tian, M., in press. Taconian retrograde eclogite from northwest
768 Connecticut, USA, and its petrotectonic implications. Lithos, doi:
769 10.1016/j.lithos.2015.10.011.

770 Condie, K.C., 1993. Chemical composition and evolution of the upper continental crust: contrasting
771 results from surface samples and shales. Chemical Geology, 104(1): 1-37.

772 Crowe, S.A. et al., 2013. Atmospheric oxygenation three billion years ago. Nature, 501(7468): 535-
773 538.

774 Dragovic, B., Samanta, L.M., Baxter, E.F., Selverstone, J., 2012. Using garnet to constrain the duration
775 and rate of water-releasing metamorphic reactions during subduction: An example from
776 Sifnos, Greece. Chemical Geology, 314: 9-22.

777 Eary, L.E., Rai, D., 1987. Kinetics of chromium (III) oxidation to chromium (VI) by reaction with
778 manganese dioxide. Environmental Science & Technology, 21(12): 1187-1193.

779 Ellis, A.S., Johnson, T.M., Bullen, T.D., 2002. Chromium isotopes and the fate of hexavalent chromium
780 in the environment. Science, 295(5562): 2060.

781 Ellis, A.S., Johnson, T.M., Bullen, T.D., 2004. Using chromium stable isotope ratios to quantify Cr (VI)
782 reduction: lack of sorption effects. Environmental Science & Technology, 38(13): 3604-
783 3607.

784 Farkas, J. et al., 2013. Chromium isotope variations ($\delta^{53/52}$Cr) in mantle-derived sources and their
785 weathering products: Implications for environmental studies and the evolution of $\delta^{53/52}$Cr in
786 the Earth's mantle over geologic time. Geochimica et Cosmochimica Acta, 123: 74-92.

787 Fendorf, S.E., Li, G., 1996. Kinetics of chromate reduction by ferrous iron. Environmental Science &
788 Technology, 30(5): 1614-1617.

789 Fendorf, S.E., Zasoski, R.J., 1992. Chromium (III) Oxidation by δ-MnO2. Environmental Science &
790 Technology, 26(1): 79-85.

791 Frei, R., Gaucher, C., Poulton, S.W., Canfield, D.E., 2009. Fluctuations in Precambrian atmospheric
792 oxygenation recorded by chromium isotopes. Nature, 461(7261): 250-253.

793 Frei, R., Poiré, D., Frei, K.M., 2014. Weathering on land and transport of chromium to the ocean in a
794 subtropical region (Misiones, NW Argentina): A chromium stable isotope perspective.
795 Chemical Geology, 381: 110-124.

796 Frei, R., Polat, A., 2012. Chromium isotope fractionation during oxidative weathering-implications
797 from the study of a Paleoproterozoic (ca. 1.9 Ga) paleosol, Schreiber Beach, Ontario, Canada.
798 Precambrian Research, 224: 434-453.

799 Furry, W., Jones, R.C., Onsager, L., 1939. On the theory of isotope separation by thermal diffusion.
800 Physical Review, 55(11): 1083.

801 Harwood, D., 1979a. Bedrock geologic map of the Norfolk quadrangle. Connecticut: US Geological
802 Survey Geological Quadrangle Maps of the United States GQ-1518, scale, 1(24,000).

803 Harwood, D.S., 1979b. Geologic map of the South Sandisfield quadrangle, Massachusetts and
804 Connecticut. Seiries Editor,

805 Huang, F. et al., 2010. Isotope fractionation in silicate melts by thermal diffusion. Nature,
806 464(7287): 396-400.

807 Izbicki, J.A., Bullen, T.D., Martin, P., Schroth, B., 2012. Delta Chromium-53/52 isotopic composition
808 of native and contaminated groundwater, Mojave Desert, USA. Applied Geochemistry, 27(4):
809 841-853.

810 Jaffe, L.A., Peucker-Ehrenbrink, B., Petsch, S.T., 2002. Mobility of rhenium, platinum group elements
811 and organic carbon during black shale weathering. Earth and Planetary Science Letters,
812 198(3): 339-353.

Jeandel, C., Minster, J., 1987. Chromium behavior in the ocean: Global versus regional processes. Global Biogeochemical Cycles, 1(2): 131-154.

Keiter, M., Ballhaus, C., Tomaschek, F., 2011. A new geological map of the Island of Syros (Aegean Sea, Greece): Implications for lithostratigraphy and structural history of the Cycladic Blueschist Unit. Geological Society of America Special Papers, 481: 1-43.

Kelley, D.S. et al., 2001. An off-axis hydrothermal vent field near the Mid-Atlantic Ridge at 30 N. Nature, 412(6843): 145-149.

Kelley, D.S. et al., 2005. A serpentinite-hosted ecosystem: the Lost City hydrothermal field. Science, 307(5714): 1428-1434.

Kim, C., Zhou, Q., Deng, B., Thornton, E.C., Xu, H., 2001. Chromium(VI) reduction by hydrogen sulfide in aqueous media: stoichiometry and kinetics. Environmental Science & Technology, 35(11): 2219-2225.

Konhauser, K.O. et al., 2011. Aerobic bacterial pyrite oxidation and acid rock drainage during the Great Oxidation Event. Nature, 478(7369): 369-373.

Krogh, E., Oh, C., Liou, J., 1994. Polyphase and anticlockwise P‐T evolution for Franciscan eclogites and blueschists from Jenner, California, USA. Journal of Metamorphic Geology, 12(2): 121-134.

Lancaster, P.J., Baxter, E.F., Ague, J.J., Breeding, C.M., Owens, T.L., 2008. Synchronous peak Barrovian metamorphism driven by syn‐orogenic magmatism and fluid flow in southern Connecticut, USA. Journal of Metamorphic Geology, 26(5): 527-538.

Lanzirotti, A., Hanson, G.N., 1996. Geochronology and geochemistry of multiple generations of monazite from the Wepawaug Schist, Connecticut, USA: implications for monazite stability in metamorphic rocks. Contributions to Mineralogy and Petrology, 125(4): 332-340.

Ling, W., Cheng, J., Wang, X., Zhou, H., 2002. Geochemical features of the Neoproterozoic igneous rocks from the Wudang region and their implications for the reconstruction of the Jinning tectonic evolution along the south Qinling orogenic belt. Acta Petrologica Sinica, 18(1): 25-36.

Malavieille, J., Chemenda, A., Larroque, C., 1998. Evolutionary model for Alpine Corsica: mechanism for ophiolite emplacement and exhumation of high-pressure rocks. Terra Nova, 10(6): 317-322.

Marschall, H.R., Schumacher, J.C., 2012. Arc magmas sourced from mélange diapirs in subduction zones. Nature Geoscience, 5(12): 862-867.

Mayanna, S. et al., 2015. Biogenic precipitation of manganese oxides and enrichment of heavy metals at acidic soil pH. Chemical Geology, 402(0): 6-17.

McDonough, W.F., Sun, S.-S., 1995. The composition of the Earth. Chemical Geology, 120(3): 223-253.

McLennan, S.M., 2001. Relationships between the trace element composition of sedimentary rocks and upper continental crust. Geochemistry, Geophysics, Geosystems, 2(4).

Middelburg, J.J., van der Weijden, C.H., Woittiez, J.R., 1988. Chemical processes affecting the mobility of major, minor and trace elements during weathering of granitic rocks. Chemical Geology, 68(3): 253-273.

Miller, C.A., Peucker-Ehrenbrink, B., Schauble, E.A., 2015. Theoretical modeling of rhenium isotope fractionation, natural variations across a black shale weathering profile, and potential as a paleoredox proxy. Earth and Planetary Science Letters, 430: 339-348.

Moynier, F., Yin, Q.-Z., Schauble, E., 2011. Isotopic evidence of Cr partitioning into Earth's core. Science, 331(6023): 1417-1420.

Page, F.Z., Armstrong, L.S., Essene, E.J., Mukasa, S.B., 2007. Prograde and retrograde history of the Junction School eclogite, California, and an evaluation of garnet–phengite–clinopyroxene thermobarometry. Contributions to Mineralogy and Petrology, 153(5): 533-555.

Papanastassiou, D., 1986. Chromium isotopic anomalies in the Allende meteorite. The Astrophysical Journal, 308: L27-L30.

Parsons, B., 1981. The rates of plate creation and consumption. Geophysical Journal International, 67(2): 437-448.

Paulick, H. et al., 2006. Geochemistry of abyssal peridotites (Mid-Atlantic Ridge, 15°20' N, ODP Leg 209): implications for fluid/rock interaction in slow spreading environments. Chemical Geology, 234(3): 179-210.

Petsch, S., Berner, R., Eglinton, T., 2000. A field study of the chemical weathering of ancient sedimentary organic matter. Organic Geochemistry, 31(5): 475-487.

Petsch, S., Eglinton, T., Edwards, K., 2001a. ^{14}C-dead living biomass: evidence for microbial assimilation of ancient organic carbon during shale weathering. Science, 292(5519): 1127-1131.

Petsch, S.T., Smernik, R., Eglinton, T., Oades, J., 2001b. A solid state ^{13}C-NMR study of kerogen degradation during black shale weathering. Geochimica et Cosmochimica Acta, 65(12): 1867-1882.

Pettine, M., D'Ottone, L., Campanella, L., Millero, F.J., Passino, R., 1998. The reduction of chromium (VI) by iron (II) in aqueous solutions. Geochimica et Cosmochimica Acta, 62(9): 1509-1519.

Planavsky, N.J. et al., 2014. Low Mid-Proterozoic atmospheric oxygen levels and the delayed rise of animals. Science, 346(6209): 635-638.

881 Podosek, F. et al., 1997. Thoroughly anomalous chromium in Orgueil. Meteoritics & Planetary
882 Science, 32(5): 617-627.

883 Qin, L. et al., 2011. Extreme ^{54}Cr-rich nano-oxides in the CI chondrite Orgueil–Implication for a late
884 supernova injection into the solar system. Geochimica et Cosmochimica Acta, 75(2): 629-
885 644.

886 Qin, L., Xia, J., Carlson, R., Zhang, Q., 2015. Chromium Stable Isotope Composition of Meteorites,
887 Lunar and Planetary Science Conference.

888 Rai, D., Eary, L., Zachara, J., 1989. Environmental chemistry of chromium. Science of the Total
889 Environment, 86(1-2): 15-23.

890 Rai, D., Sass, B.M., Moore, D.A., 1987. Chromium(III) hydrolysis constants and solubility of
891 chromium(III) hydroxide. Inorganic Chemistry, 26(3): 345-349.

892 Ratschbacher, L. et al., 2003. Tectonics of the Qinling (Central China): tectonostratigraphy,
893 geochronology, and deformation history. Tectonophysics, 366(1-2): 1-53.

894 Reinhard, C.T. et al., 2013. Proterozoic ocean redox and biogeochemical stasis. Proceedings of the
895 National Academy of Sciences of the United States of America, 110(14): 5357-5362.

896 Reinhard, C.T. et al., 2014. The isotopic composition of authigenic chromium in anoxic marine
897 sediments: A case study from the Cariaco Basin. Earth and Planetary Science Letters, 407: 9-
898 18.

899 Richter, F.M., Watson, E.B., Mendybaev, R.A., Teng, F.-Z., Janney, P.E., 2008. Magnesium isotope
900 fractionation in silicate melts by chemical and thermal diffusion. Geochimica et
901 Cosmochimica Acta, 72(1): 206-220.

902 Rotaru, M., Birck, J.L., Allegre, C.J., 1992. Clues to early solar system history from chromium isotopes
903 in carbonaceous chondrites. Nature, 358: 465-470.

904 Rudnick, R.L., Gao, S., 2003. Composition of the Continental Crust. In: Turekian, H.D.H.K. (Ed.),
905 Treatise on Geochemistry, Pergamon, Oxford, vol. 3, pp. 1-64.

906 Sawyer, D., Whitmarsh, R., Klaus, A., 1994. Iberia Abyssal Plain Sites 897-901, Proceedings of the
907 Ocean Drilling Program, Initial Reports, College Station, TX (Ocean Drilling Program), vol.
908 149.

909 Schauble, E., Rossman, G.R., Taylor, H.P., Jr, 2004. Theoretical estimates of equilibrium chromium-
910 isotope fractionations. Chemical Geology, 205(1-2): 99-114.

911 Schauble, E.A., 2007. Role of nuclear volume in driving equilibrium stable isotope fractionation of
912 mercury, thallium, and other very heavy elements. Geochimica et Cosmochimica Acta, 71(9):
913 2170-2189.

914 Scheiderich, K., Amini, M., Holmden, C., Francois, R., 2015. Global variability of chromium isotopes in
915 seawater demonstrated by Pacific, Atlantic, and Arctic Ocean samples. Earth and Planetary
916 Science Letters, 423: 87-97.

917 Schoenberg, R., Zink, S., Staubwasser, M., von Blanckenburg, F., 2008. The stable Cr isotope
918 inventory of solid Earth reservoirs determined by double spike MC-ICP-MS. Chemical
919 Geology, 249(3-4): 294-306.

920 Schwarzenbach, E.M., Frueh-Green, G.L., Bernasconi, S.M., Alt, J.C., Plas, A., 2013. Serpentinization
921 and carbon sequestration: A study of two ancient peridotite-hosted hydrothermal systems.
922 Chemical Geology, 351: 115-133.

923 Schwarzenbach, E.M. et al., 2012. Sulfur geochemistry of peridotite-hosted hydrothermal systems:
924 comparing the Ligurian ophiolites with oceanic serpentinites. Geochimica et Cosmochimica
925 Acta, 91: 283-305.

926 Seyfried, W., Foustoukos, D., Fu, Q., 2007. Redox evolution and mass transfer during
927 serpentinization: An experimental and theoretical study at 200° C, 500bar with implications
928 for ultramafic-hosted hydrothermal systems at Mid-Ocean Ridges. Geochimica et
929 Cosmochimica Acta, 71(15): 3872-3886.

930 Shen, J. et al., 2015. Chromium isotope signature during continental crust subduction recorded in
931 metamorphic rocks. Geochemistry, Geophysics, Geosystems, 16.

932 Shipboard Scientific Party, 2004. Leg 209 summary. In: Kelemen, P., Kikawa, E., Miller, D., al., e.
933 (Eds.), Proceedings of the Ocean Drilling Program, Initial Reports, College Station, TX (Ocean
934 Drilling Program), vol. 209, pp. 1-139.

935 Shukolyukov, A., Lugmair, G., 2006. Manganese–chromium isotope systematics of carbonaceous
936 chondrites. Earth and Planetary Science Letters, 250(1): 200-213.

937 Staudigel, H., 2014. Chemical Fluxes from Hydrothermal Alteration of the Oceanic Crust. In:
938 Turekian, H.D.H.K. (Ed.), Treatise on Geochemistry (Second Edition), Elsevier, Oxford, vol. 4,
939 pp. 583-606.

940 Sullivan, P.J., Yelton, J.L., Reddy, K., 1988. Iron sulfide oxidation and the chemistry of acid
941 generation. Environmental Geology and Water Sciences, 11(3): 289-295.

942 Sun, S.-S., McDonough, W., 1989. Chemical and isotopic systematics of oceanic basalts: implications
943 for mantle composition and processes. Geological Society, London, Special Publications,
944 42(1): 313-345.

945 Tebo, B.M. et al., 2004. Biogenic manganese oxides: properties and mechanisms of formation.
946 Annual Review of Earth and Planetary Sciences, 32: 287-328.

947 Terry, M.P., Robinson, P., Ravna, E.J.K., 2000. Kyanite eclogite thermobarometry and evidence for
948 thrusting of UHP over HP metamorphic rocks, Nordøyane, Western Gneiss Region, Norway.
949 American Mineralogist, 85(11-12): 1637-1650.

950 Trinquier, A., Birck, J.-L., Allègre, C.J., 2007. Widespread ^{54}Cr heterogeneity in the inner solar system.
951 The Astrophysical Journal, 655(2): 1179-1185.

952 Trinquier, A., Birck, J.-L., Allègre, C.J., 2008. High-precision analysis of chromium isotopes in
953 terrestrial and meteorite samples by thermal ionization mass spectrometry. Journal of
954 Analytical Atomic Spectrometry, 23(12): 1565-1574.

955 Trotet, F., Vidal, O., Jolivet, L., 2001. Exhumation of Syros and Sifnos metamorphic rocks (Cyclades,
956 Greece). New constraints on the PT paths. European Journal of Mineralogy, 13(5): 901-902.

957 Van der Weijden, C., van der Weijden, R.D., 1995. Mobility of major, minor and some redox-sensitive
958 trace elements and rare-earth elements during weathering of four granitoids in central
959 Portugal. Chemical Geology, 125(3): 149-167.

960 Vital Brovarone, A., Groppo, C., Hetenyi, G., Compagnoni, R., Malavieille, J., 2011. Coexistence of
961 lawsonite‐bearing eclogite and blueschist: phase equilibria modelling of Alpine Corsica
962 metabasalts and petrological evolution of subducting slabs. Journal of Metamorphic
963 Geology, 29(5): 583-600.

964 Wakabayashi, J., 1999. The Franciscan: California's classic subduction complex. Geological Society of
965 America Special Papers, 338: 111-121.

966 Wang, H. et al., 2013. Continental origin of eclogites in the North Qinling terrane and its tectonic
967 implications. Precambrian Research, 230: 13-30.

968 Wang, X.L., Johnson, T.M., Ellis, A.S., 2015a. Equilibrium Isotopic Fractionation and Isotopic
969 Exchange Kinetics between Cr (III) and Cr (VI). Geochimica et Cosmochimica Acta, 153: 72–
970 90.

971 Wang, X.L., Johnson, T.M., Lundstrom, C.C., 2015b. Isotope fractionation during oxidation of
972 tetravalent uranium by dissolved oxygen. Geochimica et Cosmochimica Acta, 150(0): 160-
973 170.

974 Wanner, C., Eggenberger, U., Kurz, D., Zink, S., Mäder, U., 2011. A chromate-contaminated site in
975 southern Switzerland, part 1: Site characterization and the use of Cr isotopes to delineate
976 fate and transport. Applied Geochemistry, 27: 644-654.

977 Whitmarsh, R.B., Beslier, M.-O., Wallace, P.J., 1998. Return to Iberia Sites 1065–1070, Proceedings of
978 the Ocean Drilling Program, Initial Reports, College Station, TX (Ocean Drilling Program),
979 vol. 173.

980 Zink, S., Schoenberg, R., Staubwasser, M., 2010. Isotopic fractionation and reaction kinetics between
981 Cr(III) and Cr(VI) in aqueous media. Geochimica et Cosmochimica Acta, 74: 5729-5745.

982

983 Table 1. Basic information and results for all samples examined in this study.

984

	Sample ID	Location	Literature	Distance from surface (m)	[Cr] (ug/g)*	δ^{53}Cr (‰)	error (‰)**	n***
NAS shale	NAS0	Kentucky, USA	Jaffe et al., 2002	0.00	107.4	0.47	0.08	2
	NAS3	"	"	0.91	93.6	0.13	0.08	2
	NAS8	"	"	2.44	89.1	0.17	0.08	2
	NAS14	"	"	4.27	77.3	0.15	0.08	2
	NAS20	"	"	6.10	74.5	-0.53	0.08	2
	NAS26	"	"	7.92	73.0	0.07	0.08	2
	NAS36	"	"	10.97	72.8	0.00	0.08	2
	NAS46	"	"	14.02	71.1	0.02	0.08	2
				Depth (mbsf)****				
Serpentinite	1268A-1	MAR 15°20' fraction zone	Paulick et al., 2006	35.4	883.3	-0.02	0.08	1
	1268A-2	"	"	82.1	1153.6	0.06	0.08	1
	1272A-5	"	Bach et al., 2004	99.4	1168.5	0.04	0.08	1
	1272A-6	"	"	107.5	792.0	0.25	0.08	1

1070A-1	Iberian Margin	Schwarzenbach et al., 2012	705.6	1250.6	0.26	0.08	2
1070A-2	"	"	706.3	1692.4	0.09	0.08	1
1070A-3	"	"	707.02	1253.3	0.09	0.08	1
1070A-3-dc*****	"	"	"	"	0.10	0.08	1
897C-3	"	Schwarzenbach et al., 2013	680	858.5	0.52	0.08	1
897C-3-dc	"	"	"	"	0.51	0.08	1
897C-7	"	"	710	595.5	0.10	0.08	1
897D-9	"	"	742.2	659.0	0.14	0.08	1
897D-13	"	"	773	980.2	0.20	0.08	1
LA3a	Cava dei Marmi	Schwarzenbach et al., 2012		1604.4	-0.11	0.08	1
LA20a	"	"		1717.5	0.12	0.08	1
LM027	Cava Montaretto	"		1951.7	-0.15	0.08	1
LM027-dc	"	"		"	-0.13	0.08	1
JAGSY12A	Syros, Greece	37° 29.607’ N, 24° 54.556’ E		2514.4	-0.18	0.08	1
JAGSY12A-dc	"	"		"	-0.16	0.08	2

	JAGSY12A-dd*****	"	"		"	-0.17	0.08	1
	JAGSY13C	"	37° 29.421’ N, 24° 54.078’ E		3037.8	-0.11	0.08	1
	JAGSY8A-2	"	Marschall et al., 2012		2454.3	-0.17	0.08	1
Altered oceanic crust	VZP	Equitorial East Pacific	Bach et al., 2003	274.5–846	316.0	-0.19	0.08	1
	VZM	"	"	"	387.1	-0.22	0.08	1
	VZB	"	"	"	264.7	-0.17	0.08	1
	TZP	"	"	"	358.2	-0.07	0.08	1
	TZM	"	"	"	360.3	-0.23	0.08	1
	TZM-dc	"	"	"	"	-0.21	0.08	1
	SDCB	"	"	> 1055	199.2	-0.20	0.08	1
	SDCD	"	"	"	333.9	-0.18	0.08	1
				Distance from vein (cm)				
MetaCarbonate	JAW-197 AS	Connecticut, USA	Ague, 2003	-1	26.3	-0.05	0.08	1
	JAW-197 AS-dc	"	"	"	"	-0.04	0.08	1
	JAW-197 Ai	"	"	0	27.8	-0.05	0.08	1

	JAW-197 Aii	"	"	3	32.2	-0.05	0.08	1
	JAW-197 Aiii	"	"	5	35.5	-0.03	0.08	1
	JAW-197 Aiii-dc	"	"	"		-0.01	0.08	1
	JAW-197 Aiv	"	"	6	35.3	-0.01	0.08	1
	JAW-197 Av	"	"	8	35.3	-0.01	0.08	1
Mafic/Metamafic	WD05-02	Hubei, China	Ling et al., 2008		136.4	-0.13	0.08	1
	WD05-07	"	"		1255.6	-0.04	0.08	1
	WD05-10	"	"		1260.3	-0.02	0.08	1
	WD05-11	"	"		1259.1	-0.03	0.08	1
	WD05-23	"	"		96.1	-0.08	0.08	1
	WD06-52	"	"		335.6	-0.12	0.08	1
	WD05-54	"	"		148.8	-0.21	0.08	1
	WD05-56	"	"		162.2	-0.20	0.08	1
	WD05-61	"	"		224.3	-0.19	0.08	1
	WD05-63	"	"		131.3	-0.13	0.08	1
	10QL136	Henan, China	Wang et al., 2013		158.1	-0.10	0.08	1
	10QL137	"	"		153.6	-0.11	0.08	1

10QL138	"	"	51.9	-0.01	0.08	1
10QL139	"	"	126.8	-0.10	0.08	1
10QL140	"	"	163.3	-0.08	0.08	2
10QL141	"	"	119.9	-0.08	0.08	1
10QL144	"	"	100.8	-0.10	0.08	1
10QL145	"	"	48.2	-0.08	0.08	2
10QL147	"	"	48.0	-0.08	0.08	1
10QL149	"	"	93.2	-0.06	0.08	1
CRB	Farinole, Corsica	Vitale Brovarone, 2011	404.6	-0.22	0.08	1
CRB-dc	"	"	"	-0.21	0.08	1
JAGTI-1A	Tinos, Greece	Broecker and Enders, 1999	62.5	-0.08	0.08	2
JAGSY-58A	Syros, Greece	37° 26.660’ N, 24° 53.327’ E	1576.6	-0.24	0.08	1
JAQ158A	Connecticut, USA	41° 52.423’ N, 72° 16.335’ W	663.3	-0.08	0.08	2
JANW-17	Connecticut, USA	Harwood, 1979a, b	50.1	-0.17	0.08	1
CBJB2	California, USA	Krogh et al., 1994	65.5	-0.16	0.08	1
6001	"	Page et al., 2007	120.8	-0.20	0.08	1

6001-dc	"	"	"	-0.14	0.08	2
4-1	Norway	Terry et al., 2000	498.8	-0.22	0.08	1

* Based on isotope dilution.

** 2 standard deviation of NIST SRM 3112a and USGS BHVO-2 that went through the same chemical procedures as samples.

*** remeasurement of the same purified sample solution

**** meters below seafloor

*****'dc' represents duplicated column chemistry; 'dd' represent duplicated digestion+column chemistry.

985

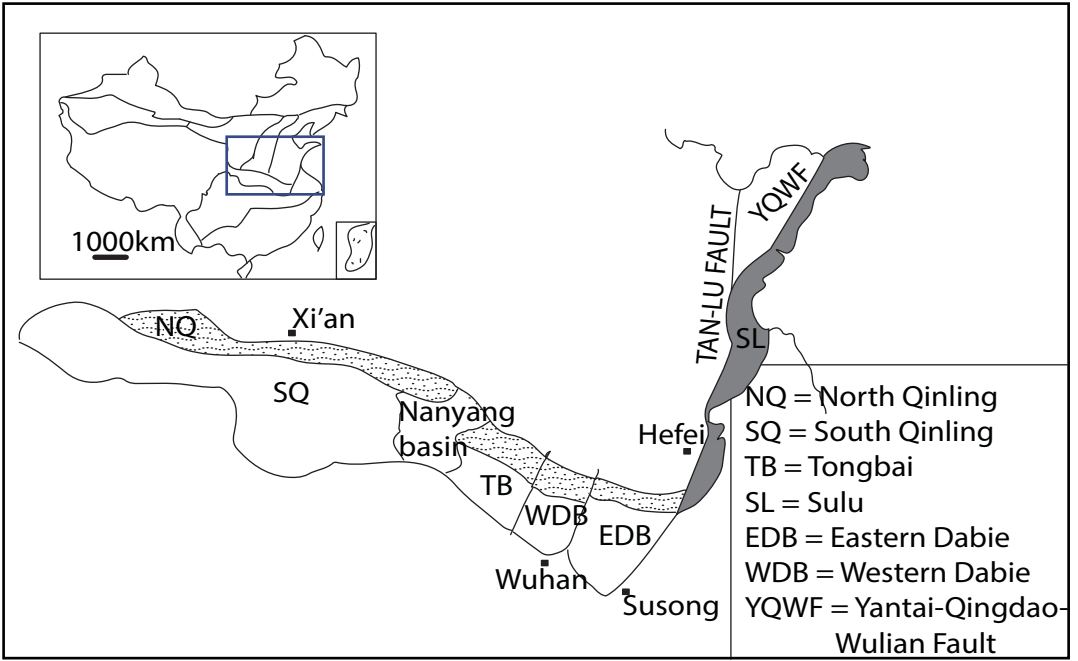
1000km
NQ
Xi'an
SQ
Nanyang
basin
TB
WDB
EDB
Wuhan
Susong
Hefei
TAN-LU FAULT
YQWF
SL
NQ = North Qinling
SQ = South Qinling
TB = Tongbai
SL = Sulu
EDB = Eastern Dabie
WDB = Western Dabie
YQWF = Yantai-Qingdao-
Wulian Fault

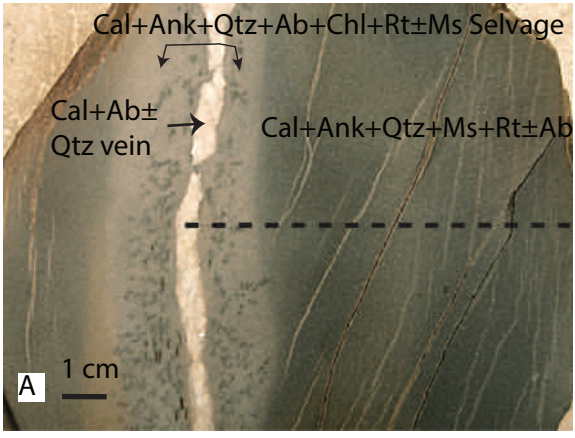
Cal+Ank+Qtz+Ab+Chl+Rt±Ms Selvage
Cal+Ab±
Qtz vein
Cal+Ank+Qtz+Ms+Rt±Ab
A
1 cm

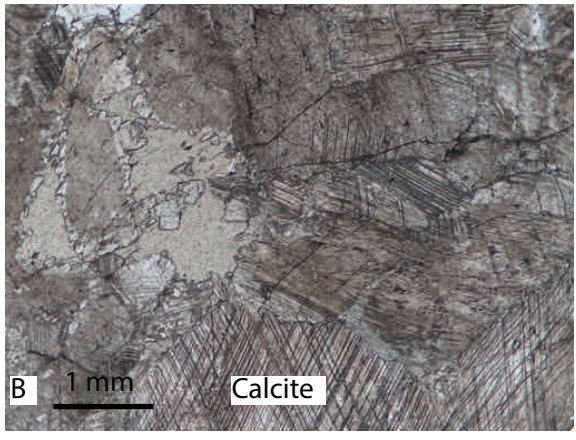
B
1 mm
Calcite

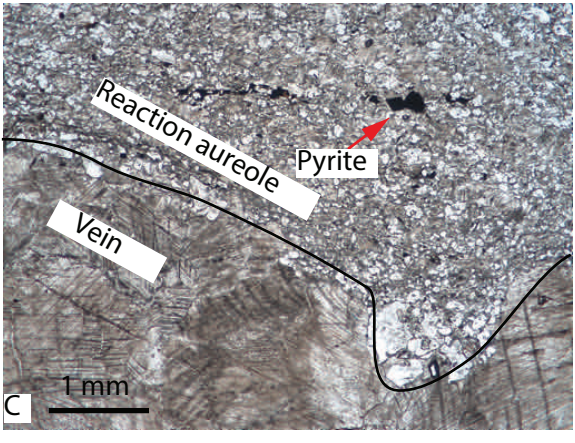
Reaction aureole
Pyrite
Vein
C
1 mm

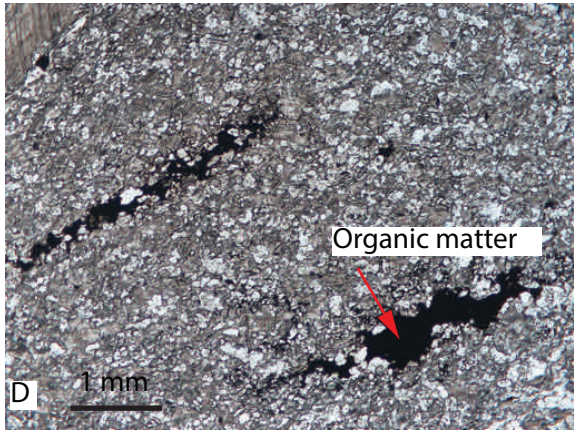
Organic matter
D
1 mm

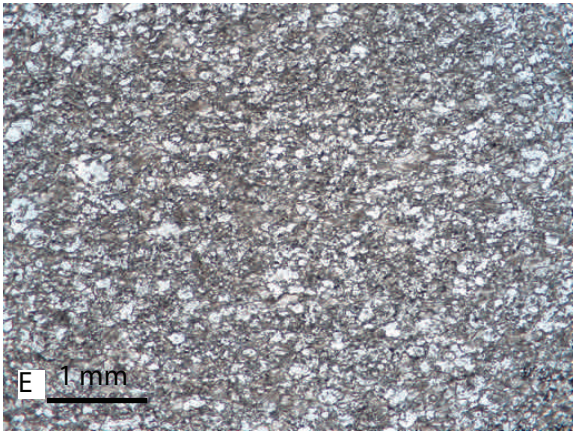
E
1 mm

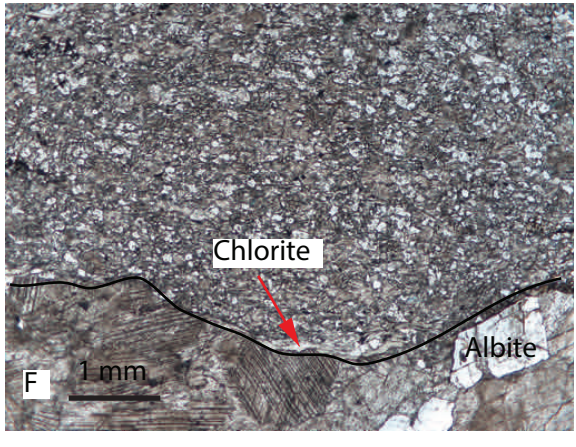
Chlorite
Albite
F
1 mm

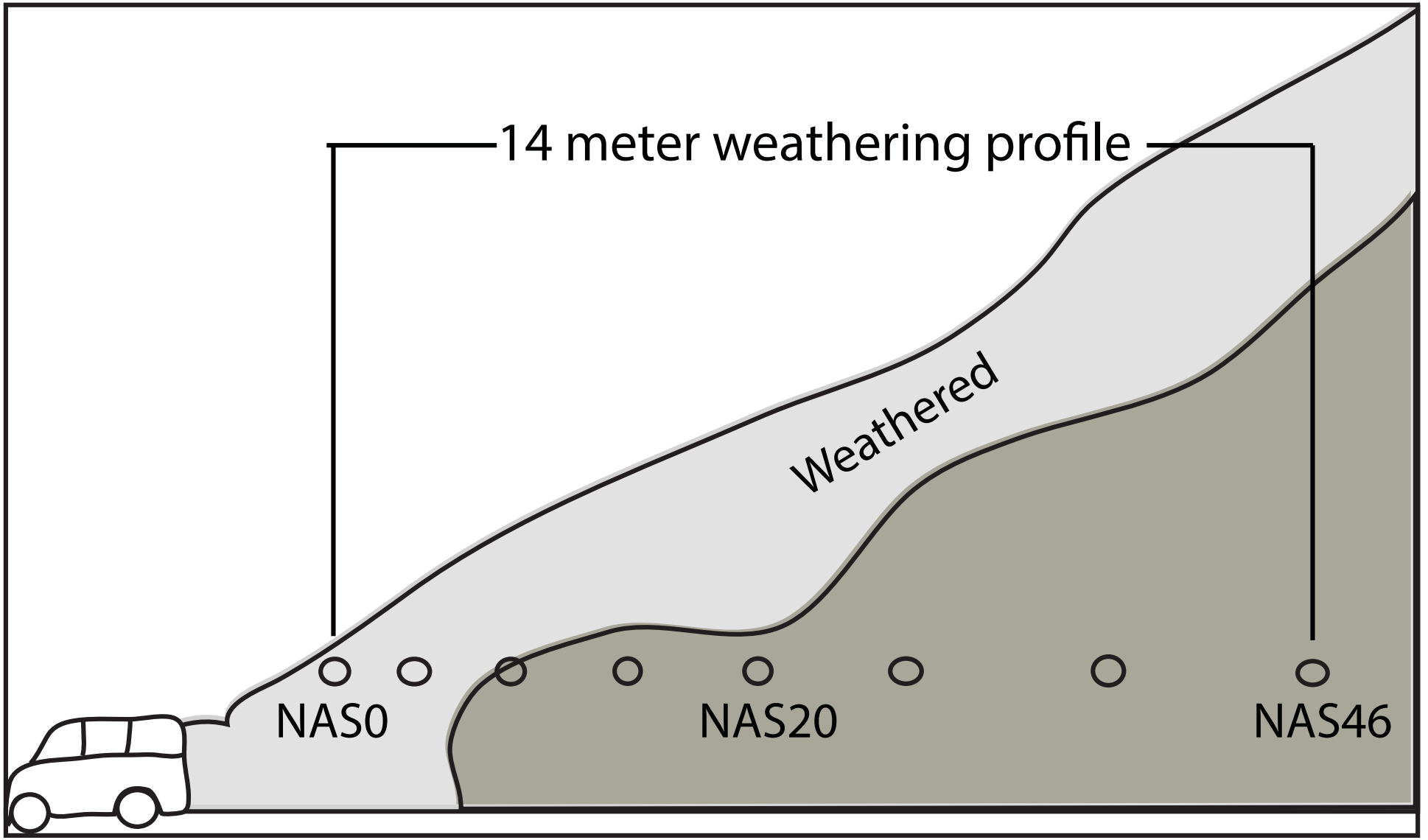
14 meter weathering profile
Weathered
NAS0
NAS20
NAS46

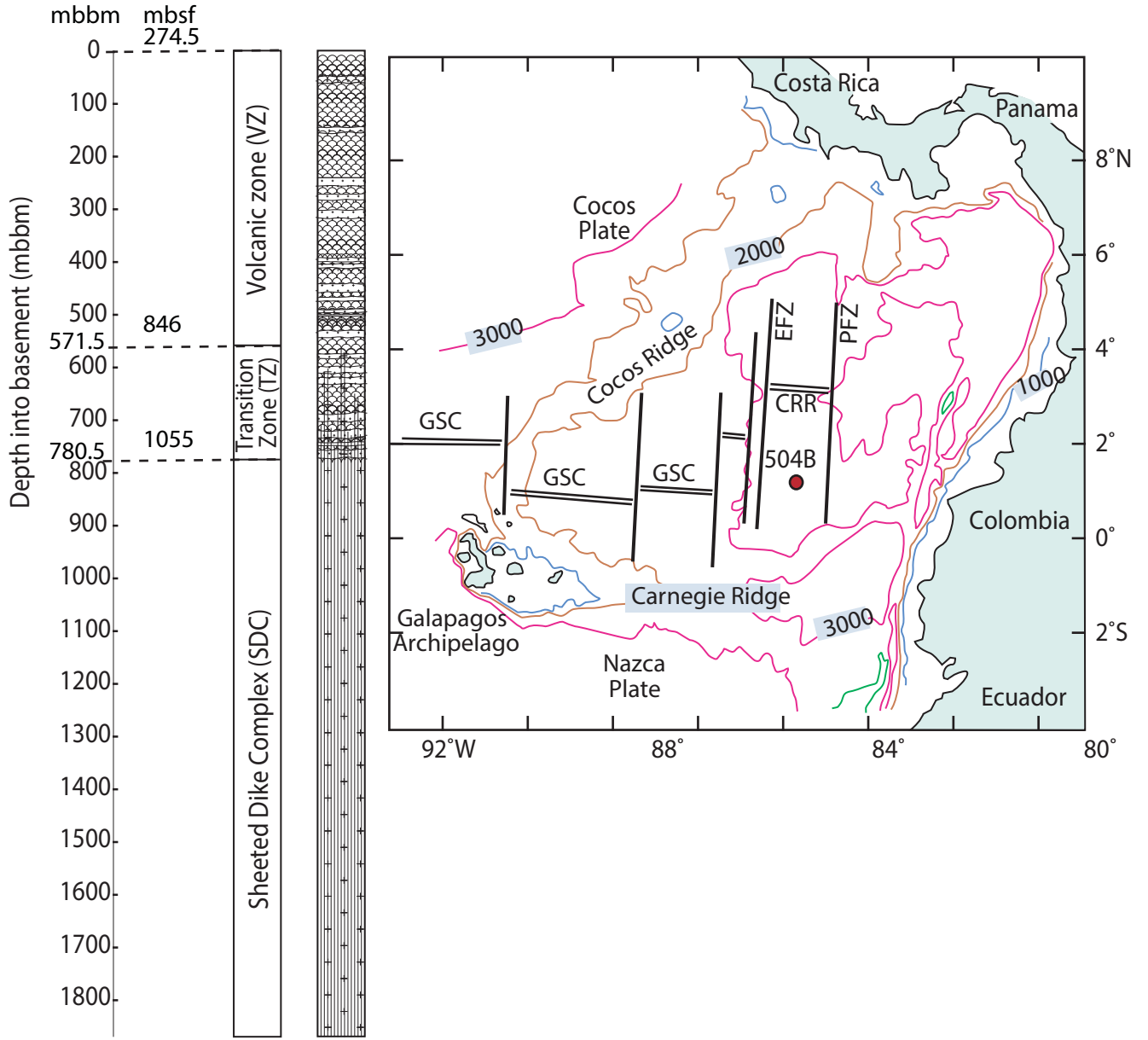
mbbm
mbsf
274.5
846
571.5
1055
780.5
Depth into basement (mbbm)
0
100
200
300
400
500
600
700
800
900
1000
1100
1200
1300
1400
1500
1600
1700
1800
Volcanic zone (VZ)
Transition Zone (TZ)
Sheeted Dike Complex (SDC)
Costa Rica
Panama
Cocos Plate
2000
3000
Cocos Ridge
EFZ
PFZ
CRR
1000
GSC
GSC
GSC
504B
Colombia
Carnegie Ridge
3000
Galapagos Archipelago
Nazca Plate
Ecuador
8°N
6°
4°
2°
0°
2°S
92°W
88°
84°
80°

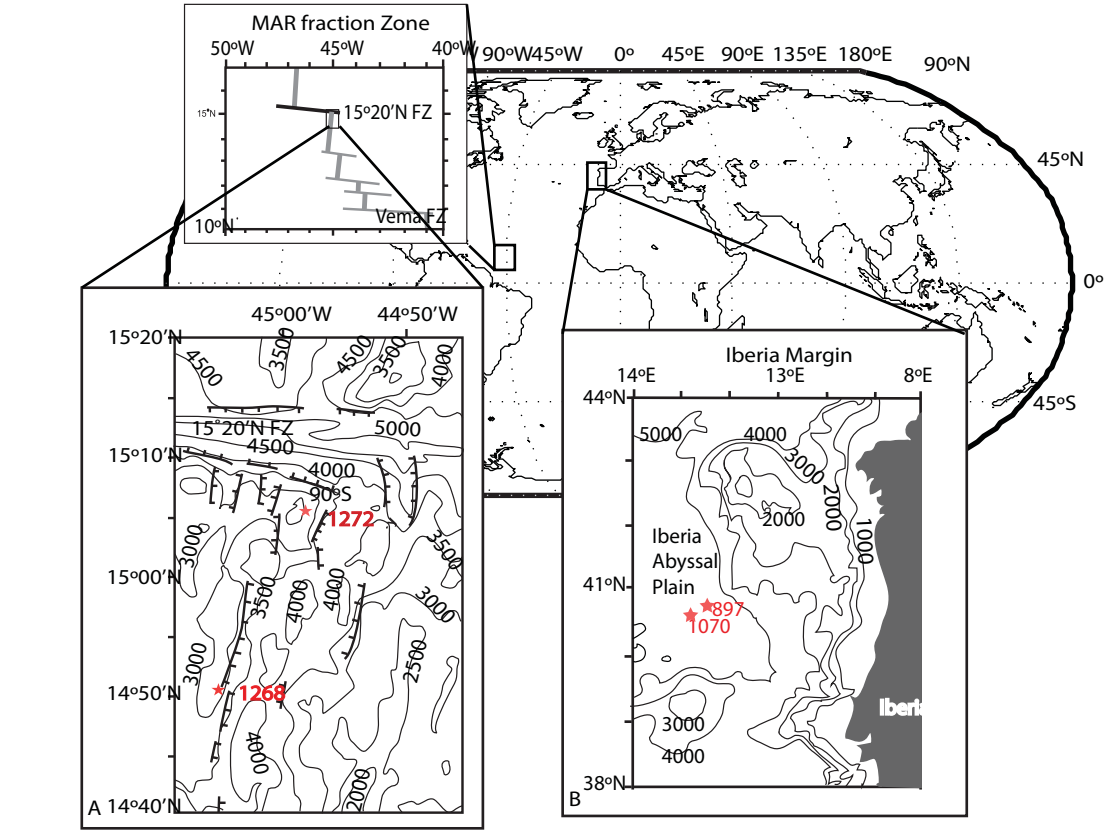
MAR fraction Zone
50°W
45°W
40°W
15°N
10°N
15°20′N FZ
Vema FZ
90°W45°W
0°
45°E
90°E
135°E
180°E
90°N
45°N
0°
45°S
45°00′W
44°50′W
15°20′N
15°10′N
15°00′N
14°50′N
14°40′N
15°20′N FZ
90°S
1272
1268
A
Iberia Margin
14°E
13°E
8°E
44°N
41°N
38°N
Iberia
Abyssal
Plain
897
1070
B

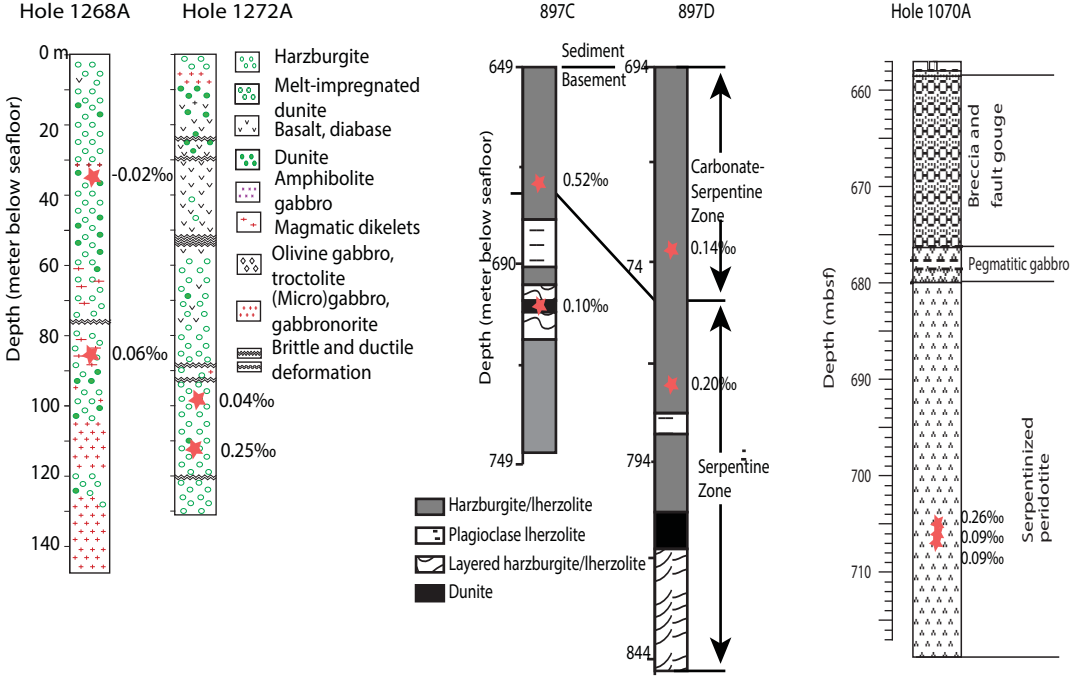
Hole 1268A
Hole 1272A
0 m
Depth (meter below seafloor)
-0.02‰
0.06‰
0.04‰
0.25‰
Harzburgite
Melt-impregnated dunite
Basalt, diabase
Dunite
Amphibolite gabbro
Magmatic dikelets
Olivine gabbro, troctolite
(Micro)gabbro, gabbronorite
Brittle and ductile deformation
C
897C
897D
Sediment
Basement
649
694
690
74
749
794
844
0.52‰
0.10‰
0.14‰
0.20‰
Carbonate-Serpentine Zone
Serpentine Zone
Harzburgite/lherzolite
Plagioclase lherzolite
Layered harzburgite/lherzolite
Dunite
D
Hole 1070A
Depth (mbsf)
660
670
680
690
700
710
Breccia and fault gouge
Pegmatitic gabbro
Serpentinized peridotite
0.26‰
0.09‰
0.09‰
E

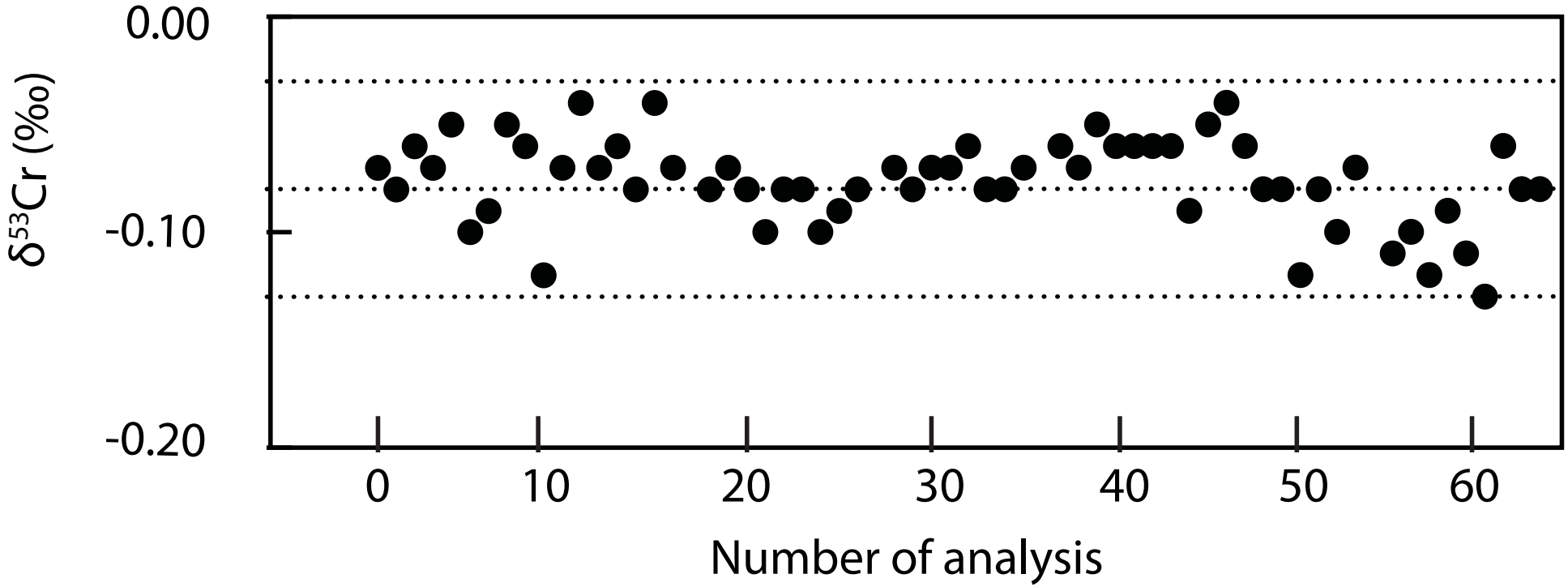
0.00
-0.10
-0.20
δ53Cr (‰)
0
10
20
30
40
50
60
Number of analysis

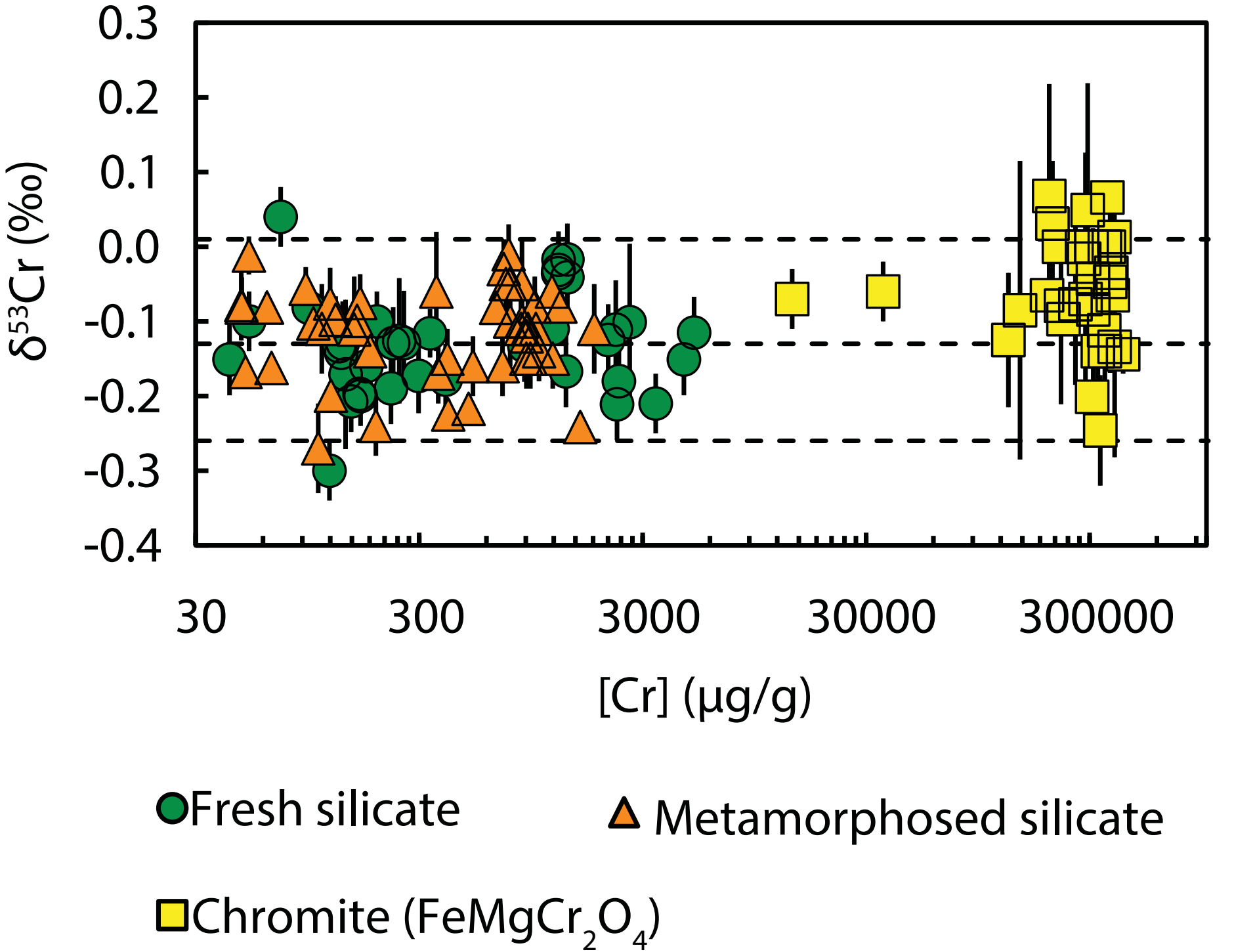
0.3
0.2
0.1
0.0
-0.1
-0.2
-0.3
-0.4
δ53Cr (‰)
30
300
3000
30000
300000
[Cr] (µg/g)
Fresh silicate
Metamorphosed silicate
Chromite (FeMgCr2O4)

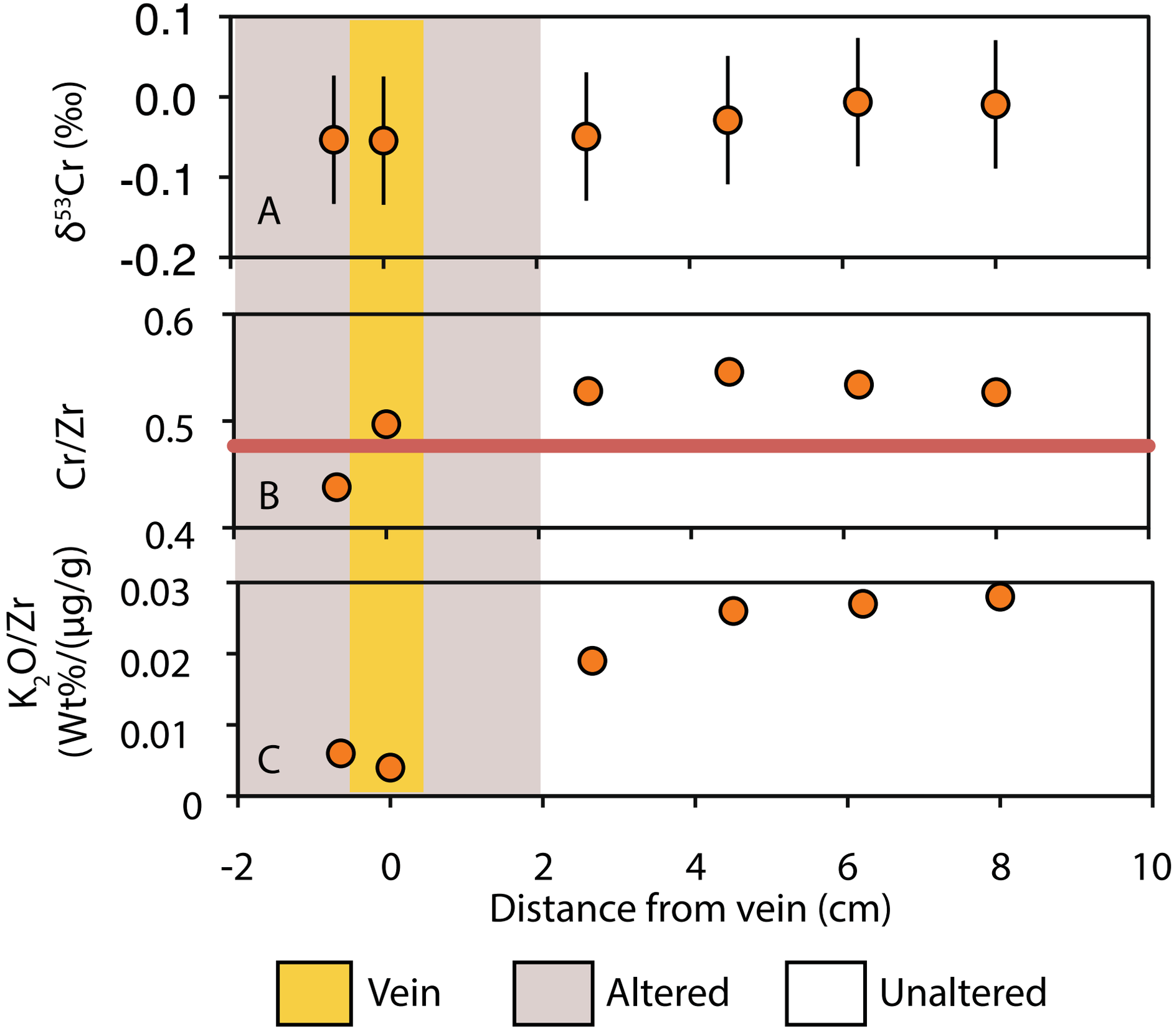
0.1
0.0
-0.1
-0.2
δ53Cr (‰)
A
0.6
0.5
0.4
Cr/Zr
B
0.03
0.02
0.01
0
K2O/Zr
(Wt%/(µg/g)
C
-2
0
2
4
6
8
10
Distance from vein (cm)
Vein
Altered
Unaltered

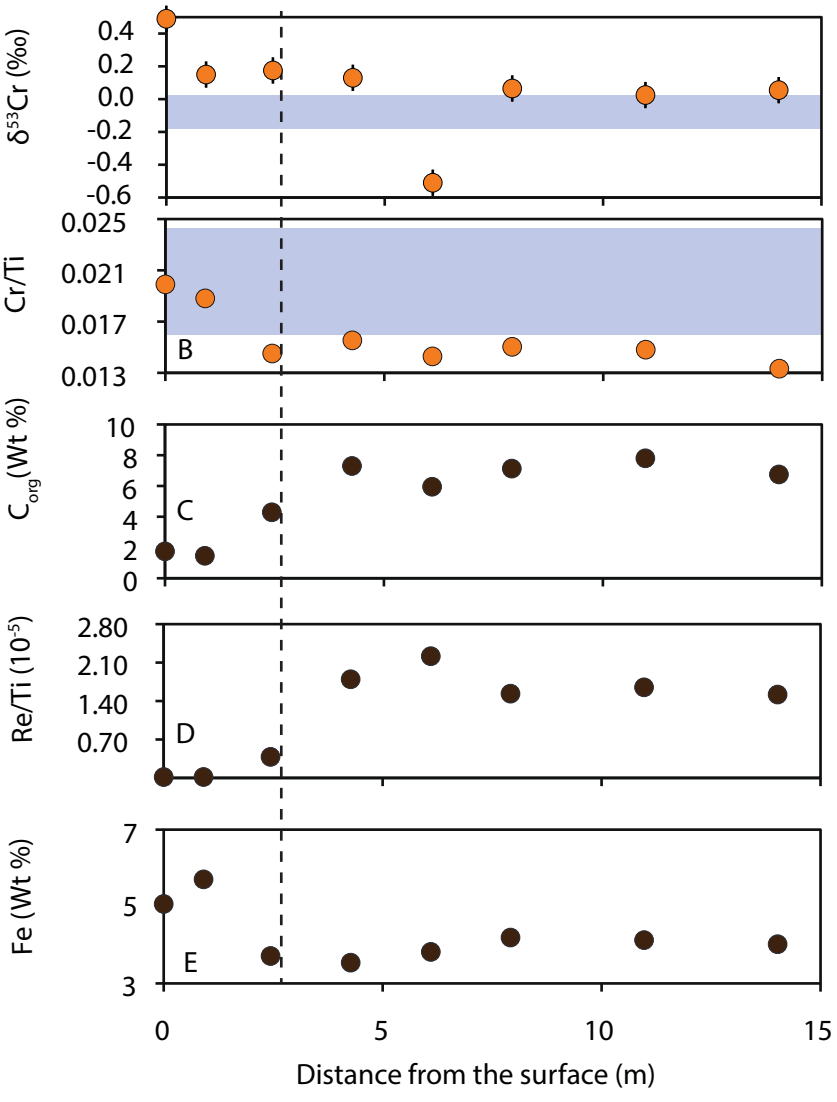
δ53Cr (‰)
0.4
0.2
0.0
-0.2
-0.4
-0.6
Cr/Ti
0.025
0.021
0.017
0.013
B
Corg (Wt %)
10
8
6
4
2
0
C
Re/Ti (10-5)
2.80
2.10
1.40
0.70
D
Fe (Wt %)
7
5
3
E
0
5
10
15
Distance from the surface (m)

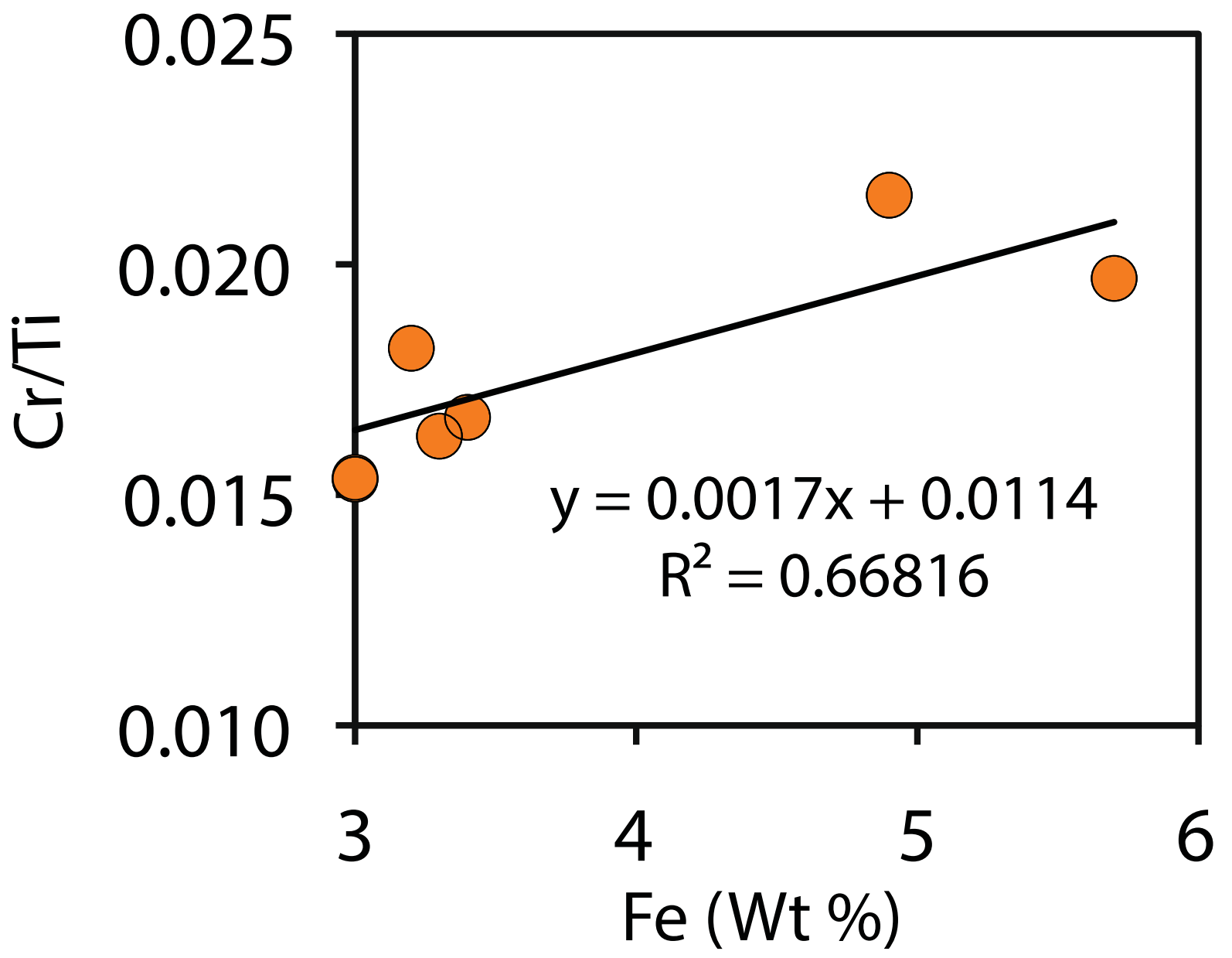
0.025
0.020
0.015
0.010
Cr/Ti
y = 0.0017x + 0.0114
R² = 0.66816
3
4
5
6
Fe (Wt %)

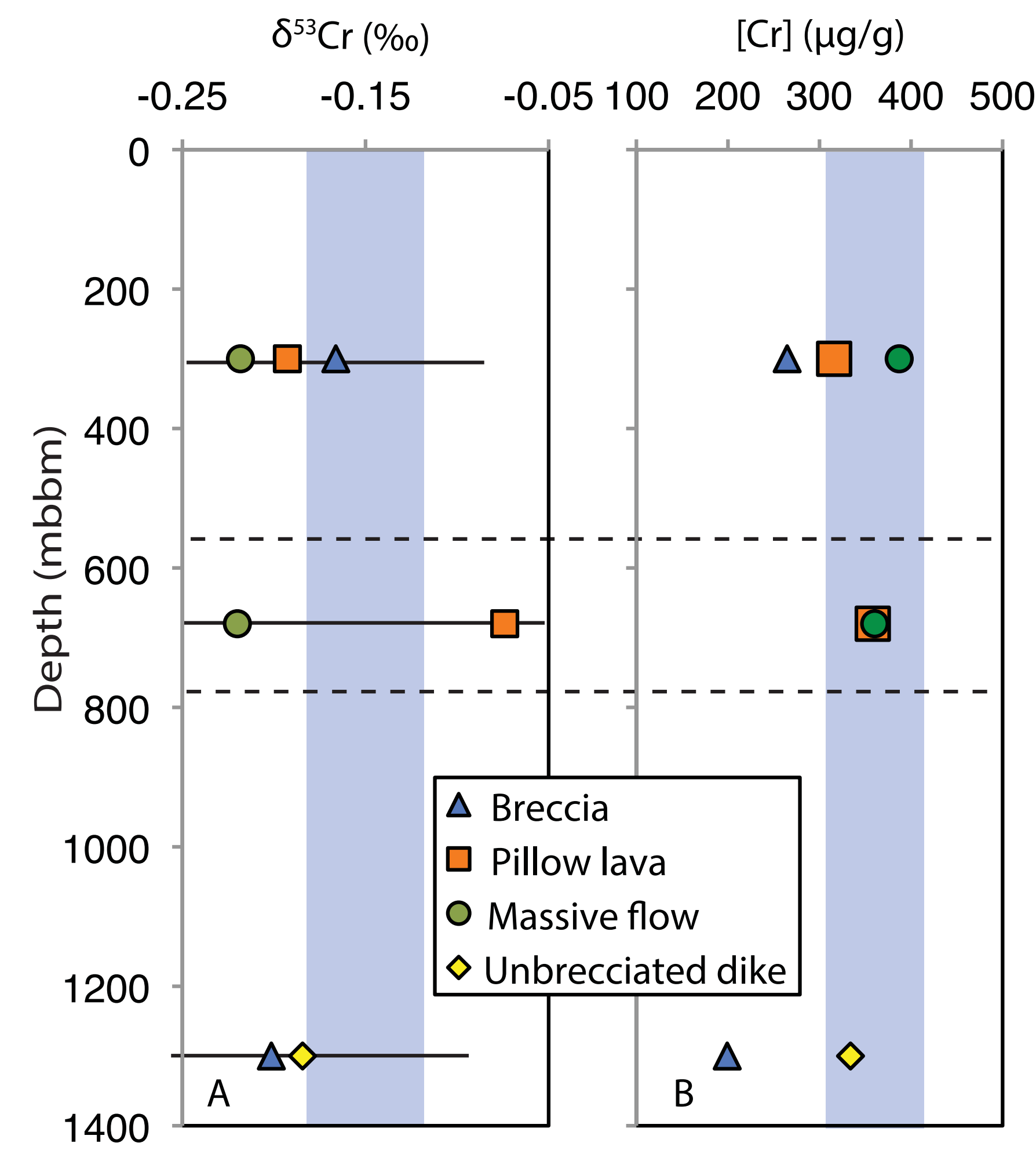
δ53Cr (‰)
[Cr] (µg/g)
-0.25
-0.15
-0.05
100
200
300
400
500
0
200
400
600
800
1000
1200
1400
Depth (mbbm)
Breccia
Pillow lava
Massive flow
Unbrecciated dike
A
B

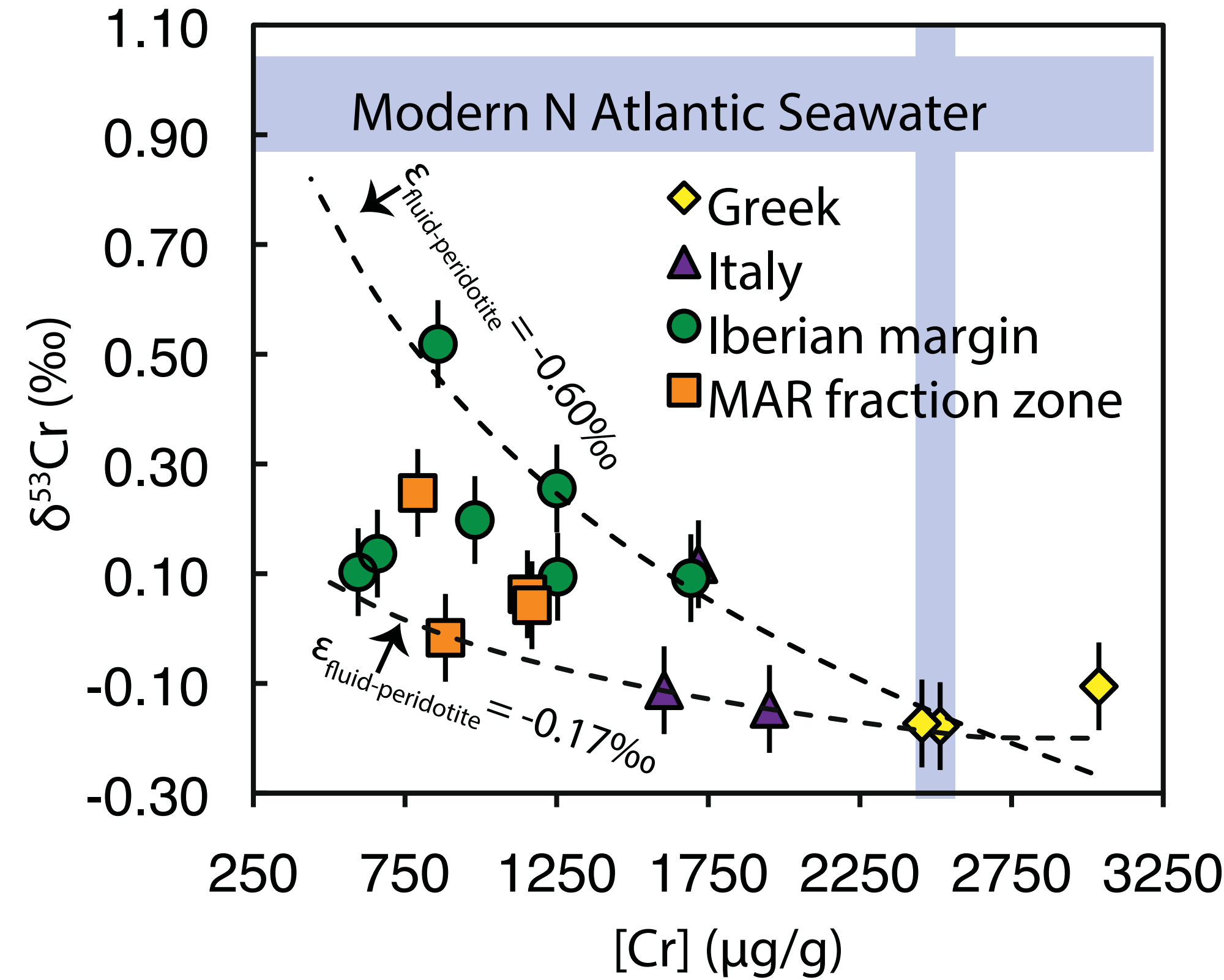
Modern N Atlantic Seawater
Greek
Italy
Iberian margin
MAR fraction zone
$\varepsilon_{fluid\text{-}peridotite} = -0.60‰$
$\varepsilon_{fluid\text{-}peridotite} = -0.17‰$
$\delta^{53}Cr$ (‰)
1.10
0.90
0.70
0.50
0.30
0.10
-0.10
-0.30
250
750
1250
1750
2250
2750
3250
[Cr] (µg/g)

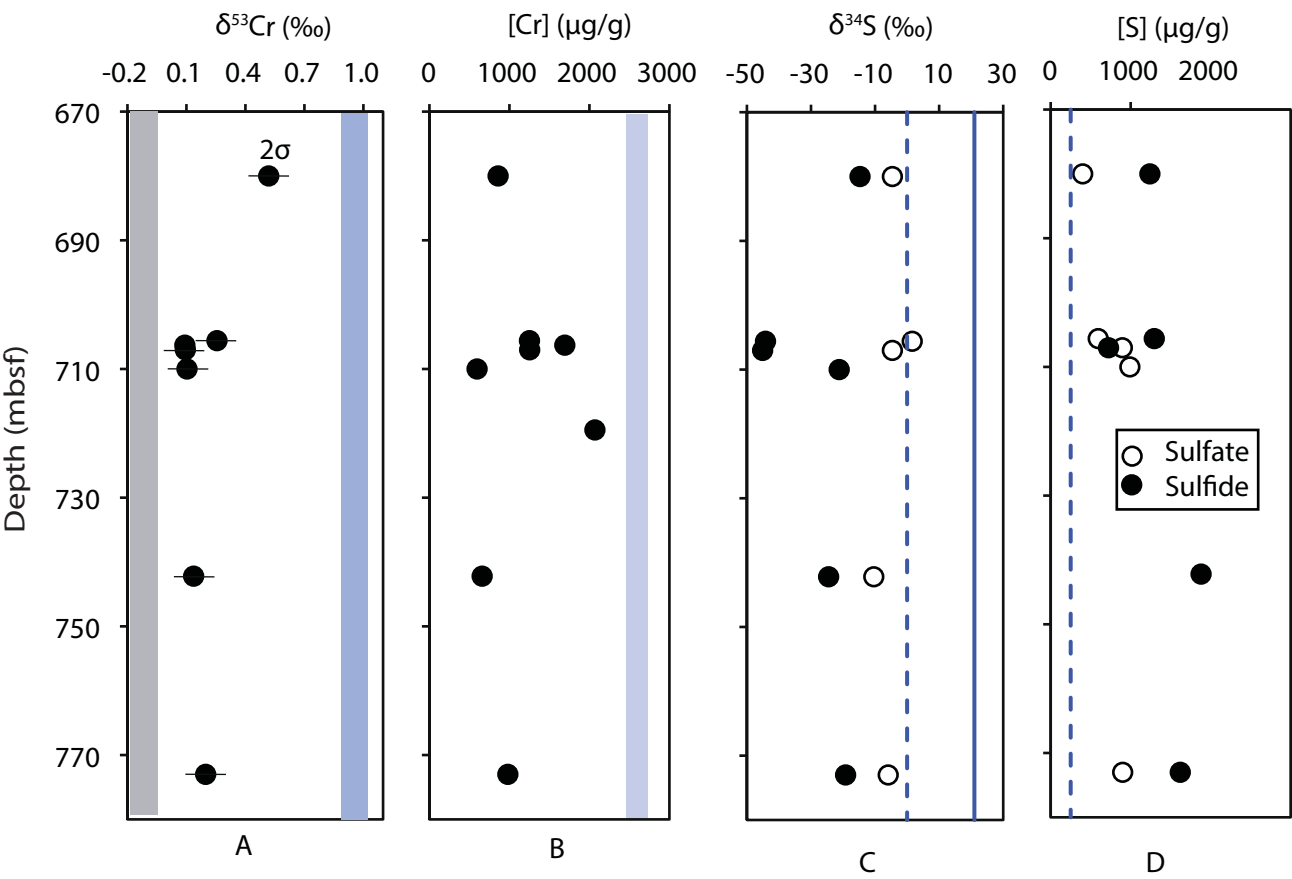
δ53Cr (‰)
-0.2 0.1 0.4 0.7 1.0
[Cr] (µg/g)
0 1000 2000 3000
δ34S (‰)
-50 -30 -10 10 30
[S] (µg/g)
0 1000 2000
Depth (mbsf)
670
690
710
730
750
770
2σ
Sulfate
Sulfide
A
B
C
D